Applications of Molecular Theory of Sum-Frequency Generations To Study Molecular Chirality†

M. Hayashi,*,‡ S. H. Lin,§ and Y. R. Shen#,⊥

Center for Condensed Matter Sciences, National Taiwan University, Taipei, 1 Roosevelt Rd. Sec. 4, 106 Taiwan, Institute of Atomic and Molecular Sciences, Academia Sinica, P.O. Box 23-166, Taipei 106 Taiwan, Department of Physics, University of California, Berkeley, California 94720, and Materials Sciences Division, Lawrence Berkeley National Laboratory, Berkeley, California 94720

Received: February 18, 2004; In Final Form: May 29, 2004

Theoretical expressions for sum-frequency generation (SFG) signals, which can be applied to treat various SFG experiments, have been derived. We have applied the theoretical results to study the SFG experiments for the near-electronic resonant, singly resonant IR−UV, and doubly resonant IR−UV cases that are associated with the measurements reported by Shen's group. We have taken into account both the electric and magnetic dipole interactions and the applied laser and detection polarization combinations explicitly. Relationships between the polarization combinations and the electric-dipole−electric-dipole mechanism, the electric-dipole−magnetic-dipole mechanism, the magnetic-dipole−electric-dipole mechanism, and the magnetic-dipole−magnetic-dipole mechanisms are clarified. Based on the theoretical results, near-electronic resonant SFG, singly resonant IR−UV SFG, doubly resonant IR SFG experiments are discussed.

1. Introduction

The adsorption of proteins from solution onto solid surfaces has attracted much attention, because of their scientific importance and applications in many areas. In medical and food processing industries, it is usually required to remove adsorbed proteins, because even a small amount of deposited protein may give rise to the subsequent adsorption of fibrous proteins, leading to adverse biological consequences.[1−3] On the other hand, controlled immobilization of proteins is crucial in the field of biotechnology, where well-ordered protein layers may lead to a new generation of reactor beds for catalysis, biosensors, and disease diagnostics.[4−6] The interaction between proteins and underlying solid substrates generally dictates the adsorption affinity, as well as the structure of adsorbed protein via denaturation, leading some amino acid residues to adopt a preferred orientation. One can use advanced nonlinear optical spectroscopies, such as sum-frequency generation (SFG), second-generation harmonics (SHG), and surface-enhanced Raman scattering (SERS), which are surface-sensitive and present many advantages.[7,8] The main drawback of the method is the very low efficiency of the SHG and SFG processes at the interface. However, by tuning the wavelength of the SHG and SFG signal on an electronic transition and/or a vibrational transition of the compounds sitting at the interface, resonance enhancement of the SHG and SFG signal compensates for this problem.

For almost two decades, infrared−ultraviolet (or visible) SFG vibrational spectroscopy, which was pioneered by Y. R. Shen and his group, has been used to extract information on surface structures from small molecules such as water, acetonitrile, carbon monoxide, etc. to large molecules such as self-assembled monolayers, polymers, and proteins at various interfaces.[9−15] Recently, the applications of nonlinear optical techniques such as SHG and SFG to probe molecular chirality have attracted considerable attention.[16−19] It is the purpose of this paper to show how to apply the molecular theory of SFG to study the molecular chirality in solution.

In SFG studies of molecular chirality, the polarization combinations of SFG experiments have an important role. In particular, inclusion of higher-order multipolar contributions to the interaction Hamiltonian[20] and the polarizabilities[21] is needed to study how magnetic-dipole and electric-quadrupole interactions are related to SFG studies of molecular chirality. Recently, Fischer et al. noted the importance of the lowest-order correction to the electric-dipole approximation (i.e., a magnetic-dipole transition moment and an electric-quadrupole transition moment) for an achiral origin of SFG.[22,23] More recently, they have observed achiral signals that are above the noise level and proposed that the origin of these signals are due to either electric-dipolar surface nonlinearities or the magnetic-dipolar/electric-quadrupolar bulk susceptibilities..[23] In addition, based on the multipolar hyperpolarizabilities, they have presented a theoretical expression of the isotropic components of the total second-order induced polarization that includes the contributions from the magnetization and electric quadrupole moment per unit volume, as well as the magnetic dipolar transition moment and the electric quadrupole transition dipole moment.

In this paper, we shall study the SFG beyond the dipole−dipole approximation, e.g., the dipole−magnetic-dipole approximation and the magnetic-dipole−magnetic-dipole approximation. For this purpose, we shall focus on induced second-order electric polarization. We will provide molecular-theoretical expressions of singly electronically resonant SFG, doubly resonant and singly resonant IR−UV SFG with the description of polarization dependence.

† Part of the special issue "Richard Bersohn Memorial Issue".

* Author to whom corespondence should be addressed. Telephone: 886-2-33665250. Fax: 886-2-23655404. E-mail address: atmyh@ccms.ntu.edu.tw.
‡ National Taiwan University.
§ Academia Sinica.
# University of California.
⊥ Lawrence Berkeley National Laboratory.

10.1021/jp0492467 CCC: $27.50
Published on Web 07/24/2004

A molecular theory of the doubly resonant and singly resonant IR−UV SFG of molecules on surfaces has been developed.[24,25] For comparison, in this paper, we shall extend this theory to study this doubly resonant SFG of chiral molecules in solution; in the Condon approximation, this nonlinear optical activity is forbidden in the dipole−dipole approximation. The Herzberg−Teller theory will be used to study the non-Condon effect on this SFG; we shall also study the effect of the breakdown of the Born−Oppenheimer adiabatic approximation on this nonlinear optical activity in solution.

Recently, the electronically singly resonant SFG of 1,1′-bi-2-naphthol (BN) in solution has been observed and measured by Shen and co-workers.[18] It is found that the chiral nonlinearity of BN is ∼2 orders of magnitude larger than the values predicted from ab initio calculations for small chiral molecules such as propylene oxide and monofluoro-oxirane.[19] This type of nonlinear optical activity is allowed in the dipole−dipole approximation. Within the electric-dipole approximation, the magnitudes and directions of the electronic transition moments are the key data that determines the nonlinear optical activity of chiral molecules in solution. We shall perform density functional theory (DFT) calculations combined with a semiempirical molecular orbital method such as ZINDO/S to determine the energy structure of the electronically excited states of BN and the electronic transition dipole moments between numerous electronically excited states (including the resonance condition) and the ground state, which will be used to calculate the nonlinear optical activity.

Note that, to compute the nonlinear optical activity involved in the singly resonant and doubly resonant IR−UV SFGs, which are forbidden in the dipole−dipole approximation, energy structures and electronic and magnetic transition moments, as well as vibronic couplings, must be calculated for numerous excited electronic states. The computation of vibronic couplings is complicated; thus, the quantitative analysis of these two SFG experiments will not be presented in this paper.

2. Optical Studies on Molecular Chirality−Linear Circular Dichroism

Although the main focus of this paper is on the SFG studies of molecular chirality, for comparison, we shall first present the theoretical treatment of linear circular dichroism (CD).[16,26−31] Note that the linear optical rotatory dispersion (ORD) is related to CD by the Kronig−Kramers transform.

The equation of motion of the density operator of the molecular system interacting with the laser fields and the heat bath is given by[32]

$$\frac{\partial\hat{\rho}}{\partial t} = -i\hat{L}_0\hat{\rho} - i\hat{L}'(t)\hat{\rho} - \hat{\Gamma}\hat{\rho} \tag{2-1}$$

where $\hat{\rho}$ denotes the density matrix (or operator) of the system, $\hat{\Gamma}$ is the damping operator due to the interaction between the system and heat bath, and $\hat{L}_0$ and $\hat{L}'(t)$ respectively represent the Liouville operators for the zeroth-order Hamiltonian and the perturbation Hamiltonian for the interaction between the system and radiation field.

In the interaction picture, $\hat{\rho} = \exp(-it\hat{L}'_0)\hat{\sigma}$, with $i\hat{L}'_0 = i\hat{L}_0 + \hat{\Gamma}$ and $\bar{L}'(t) = \exp(it\hat{L}'_0)\hat{L}'\exp(-it\hat{L}'_0)$, and eq 2-1 becomes

$$\hat{\sigma}(t) = \hat{\sigma}_i - i\int_{t_i}^{t} d\tau\bar{L}'(\tau)\hat{\sigma}(\tau) \tag{2-2}$$

where $\hat{\sigma}_i$ denotes the value of $\hat{\sigma}$ at t_i. Using the perturbation method, we obtain

$$\hat{\sigma}^{(1)}(t) = -i\int_{t_i}^{t} d\tau_1\bar{L}'(\tau_1)\hat{\sigma}_i \tag{2-3a}$$

$$\hat{\sigma}^{(2)}(t) = (-i)^2\int_{t_i}^{t} d\tau_1\int_{t_i}^{\tau_1} d\tau_2\bar{L}'(\tau_1)\bar{L}'(\tau_2)\hat{\sigma}_i \tag{2-3b}$$

etc., and, for example, the linear polarization can be expressed as

$$\vec{P}^{(1)}(t) = Tr(\vec{\mu}\hat{\rho}^{(1)}) = \sum_k\sum_l \exp(-it\omega'_{kl})\vec{\mu}_{lk}\sigma_{kl}^{(1)}(t) \tag{2-4}$$

where

$$\sigma_{kl}^{(1)}(t) = \frac{i}{\hbar}\Delta\sigma_i(kl)\int_{t_i}^{t} d\tau_1\exp(-it\omega'_{kl})V_{kl}(\tau_1) \tag{2-5}$$

and

$$\Delta\sigma_i(kl) \equiv \Delta\sigma_i(kk,ll) \equiv (\hat{\sigma}_i)_{kk} - (\hat{\sigma}_i)_{ll} \tag{2-6}$$

Here, $(\hat{\sigma}_i)_{kk}$ and $(\hat{\sigma}_i)_{ll}$ represent the equilibrium distributions of k and l states, respectively.

Let us introduce the interaction Hamiltonian, which includes both electric-dipole and magnetic-dipole approximations:

$$\hat{V}(t) = -\vec{\mu}\cdot\vec{E}(t) - \vec{M}\cdot\vec{B}(t) \tag{2-7}$$

For simplicity, the pulse-shape effect will be ignored:

$$\hat{V}(t) = -\vec{\mu}\cdot[\vec{E}^0\exp(-it\omega) + \vec{E}^{0*}\exp(it\omega)] - \vec{M}\cdot[\vec{B}^0\exp(-it\omega) + \vec{B}^{0*}\exp(it\omega)] \tag{2-8}$$

The relation between the electric and magnetic fields is given, using the Maxwell equation, $\vec{\nabla}\times\vec{E} = -\partial\vec{B}/\partial t$ [MKS], by

$$\vec{B}^0 = \frac{1}{c}(\hat{k}\times\vec{E}^0) = \frac{1}{c}|\vec{E}^0|\hat{b} = |\vec{B}^0|\hat{b} \tag{2-9}$$

where $\hat{k}$ and $\hat{b}$ represent the unit vectors of the wave vector and the magnetic field, respectively.

For left/right-hand circularly polarized lights, we have

$$\vec{E}_{L/R} = \vec{E}^0_{L/R}\exp(-it\omega) + \vec{E}^{0*}_{L/R}\exp(it\omega) \tag{2-10}$$

where

$$\frac{\vec{E}^0_{L/R}}{|\vec{E}^0|} = \hat{e}_{L/R} \tag{2-11a}$$

$$\frac{\vec{E}^{0*}_{L/R}}{|\vec{E}^0|} = \hat{e}^*_{L/R} \tag{2-11b}$$

and $\hat{e}_r$ denotes the unit polarization vector of the electric field,

$$\hat{e}_{L/R} = \frac{\hat{e}_X \pm i\hat{e}_Y}{\sqrt{2}} \tag{2-12}$$

assuming that the wave vector is parallel to the Z-axis.

In the presence of $\hat{V}$, we can calculate the rate of energy absorption by the system, using the relation[32]

$$Q_{L/R} = \left\langle\frac{\partial\hat{H}_{L/R}}{\partial t}\right\rangle = \left\langle\frac{\partial\hat{V}_{L/R}}{\partial t}\right\rangle = -\langle\vec{\mu}'_{L/R}\rangle\cdot\frac{d\vec{E}_{L/R}}{dt} = -\vec{P}'^{(1)}_{L/R}(t)\cdot\frac{d\vec{E}_{L/R}}{dt} \tag{2-13}$$

where

$$\vec{\mu}'_{\mathrm{L/R}} = \vec{\mu} \mp \left(\frac{i}{c}\right)\vec{M} \tag{2-14}$$

for an isotropic system, we obtain

$$\langle \Delta Q \rangle = \langle Q_{\mathrm{L}} \rangle - \langle Q_{\mathrm{R}} \rangle = \frac{8\omega}{3\hbar c}|\vec{E}^0|^2 \mathrm{Im}\left[\sum_k \sum_l \frac{\Delta\sigma_i(lk)}{\omega'_{kl} - \omega} R_{lk}\right] \tag{2-15}$$

where $R_{lk} = \mathrm{Im}[\vec{\mu}_{lk} \cdot \vec{M}_{kl}]$ represents the so-called rotational strength. Here, we have assumed that $\omega_{kl} > 0$ and $\omega \approx \omega_{kl}$, and an orientational average is performed in eq 2-15.

For molecular systems, we can use the B−O adiabatic approximation, $l \rightarrow av$, $k \rightarrow bu$, i.e.,

$$\langle \Delta Q \rangle = \frac{8\omega}{3\hbar c}|\vec{E}^0|^2 \sum_v \sum_u P_{av} \frac{\gamma_{bu,av}}{(\omega_{bu,av} - \omega)^2 + \gamma_{bu,av}^2} R_{av,bu} \tag{2-16}$$

where av and bu represent the vibronic manifolds and P_{av} denotes the Boltzmann distribution, i.e., $\Delta\sigma_i(av,bu) \approx (\hat{\sigma}_i)_{av,av} = P_{av}$. Notice that

$$R_{av,bu} = \mathrm{Im}[\vec{\mu}_{av,bu} \cdot \vec{M}_{bu,av}] = \mathrm{Im}[\langle \Theta_{av}|\vec{\mu}_{ab}|\Theta_{bu}\rangle \cdot \langle \Theta_{bu}|\vec{M}_{ba}|\Theta_{av}\rangle] \tag{2-17}$$

where $\vec{\mu}_{ab}$ and $\vec{M}_{ba}$ represent the electronic transition dipole and magnetic transition dipole moments, respectively. For allowed electronic transitions, eq 2-17 becomes

$$R_{av,bu} = \mathrm{Im}[\vec{\mu}_{av,bu} \cdot \vec{M}_{bu,av}] = R_{ba}|\langle \Theta_{av}|\Theta_{bu}\rangle|^2 \tag{2-18}$$

where $R_{ba} = \mathrm{Im}[\vec{\mu}_{ab} \cdot \vec{M}_{ba}]$, representing the electronic rotational strength.

That is, in this case, the band shape function of CD is the same as that of the optical absorption spectra.

3. Optical Studies on Molecular Chirality Using Sum-Frequency Generation

From section 2, we can see that the magnetic-dipole contribution has a very important role in CD and ORD studies of chiral molecules. In the theoretical treatment of SFG, it is essential to calculate the second-order nonlinear polarization and, in general, the total second-order nonlinear polarization vector consists of the electric dipolar contribution $\vec{P}^{(2)}(t)$, the magnetization, and electric quadrupole moment per unit volume.[23]

In this study, we shall focus on the electric and magnetic dipole contributions to SFG. The second-order nonlinear electric polarization vector generally can be expressed as[33−36]

$$\vec{P}^{(2)}(t) = \mathrm{Tr}\{\hat{\rho}^{(2)}(t)\vec{\mu}\} = \sum_k \sum_l \exp(-it\omega'_{kl})\vec{\mu}_{lk}\sigma_{kl}^{(2)}(t)$$

$$= \frac{(-i)^2}{\hbar^2}\int_{t_i}^{t} \mathrm{d}\tau_1 \int_{t_i}^{\tau_1} \mathrm{d}\tau_2 \sum_k \sum_{k'} \sum_l \exp(-it\omega'_{kl})\vec{\mu}_{lk} \times \{\bar{V}_{kk'}(\tau_1)\bar{V}_{k'l}(\tau_2)\Delta\sigma_i(lk') - \bar{V}_{kk'}(\tau_2)\bar{V}_{k'l}(\tau_1)\Delta\sigma_i(k'k)\}$$

$$= \vec{P}_1^{(2)}(t) + \vec{P}_2^{(2)}(t) \tag{3-1}$$

where, for example,

$$\bar{V}_{kk'}(t_1) = \exp(it_1\omega'_{kk'})V_{kk'}(t_1) \tag{3-2}$$

Let us first treat $\vec{P}_1^{(2)}(t)$. If we let

$$\hat{V}(t) = \sum_p (\hat{V}_{p+}\exp(it\omega_{\mathrm{p}}) + \hat{V}_{p-}\exp(-it\omega_{\mathrm{p}})) \tag{3-3}$$

where

$$\hat{V}_{p+} = -(\vec{\mu} \cdot \vec{E}_p^{0*} + \vec{M} \cdot \vec{B}_p^{0*}); \; \hat{V}_{p-} = -(\vec{\mu} \cdot \vec{E}_p^{0} + \vec{M} \cdot \vec{B}_p^{0}) \tag{3-4}$$

we then obtain, for SFG,

$$\vec{P}_1^{(2)}(t) = \frac{(-i)^2}{\hbar^2}\sum_k \sum_{k'} \sum_l \exp(it\omega'_{kl})\vec{\mu}_{lk}\Delta\sigma_i(lk')\sum_q \sum_p \left\{(\hat{V}_{q+})_{kk'} (\hat{V}_{p+})_{k'l} \frac{\exp[it(\omega'_{k'l} + \omega'_{kk'} + \omega_q + \omega_p)]}{i(\omega'_{k'l} + \omega_p)i(\omega'_{k'l} + \omega'_{kk'} + \omega_q + \omega_p)} + (\hat{V}_{q-})_{kk'}(\hat{V}_{p-})_{k'l} \frac{\exp[it(\omega'_{k'l} + \omega'_{kk'} - \omega_q - \omega_p)]}{i(\omega'_{k'l} - \omega_p)i(\omega'_{k'l} + \omega'_{kk'} - \omega_q - \omega_p)}\right\}$$

$$= \vec{P}_{1+}^{(2)}(t) + \vec{P}_{1-}^{(2)}(t) \tag{3-5}$$

Similarly, for $\vec{P}_2^{(2)}(t)$, we obtain, for SFG,

$$\vec{P}_2^{(2)}(t) = -\frac{(-i)^2}{\hbar^2}\sum_k \sum_{k'} \sum_l \exp(-it\omega'_{kl})\vec{\mu}_{lk}\Delta\sigma_i(k'k)\sum_q \sum_p \left\{(\hat{V}_{q+})_{k'l}(\hat{V}_{p+})_{kk'} \frac{\exp[it(\omega'_{kk'} + \omega'_{k'l} + \omega_q + \omega_p)]}{i(\omega'_{kk'} + \omega_p)i(\omega'_{kk} + \omega'_{k'l} + \omega_q + \omega_p)} + (\hat{V}_{q-})_{k'l}(\hat{V}_{p-})_{kk'} \frac{\exp[it(\omega'_{kk'} + \omega'_{k'l} - \omega_q - \omega_p)]}{i(\omega'_{kk'} - \omega_p)i(\omega'_{kk'} + \omega'_{k'l} - \omega_q - \omega_p)}\right\}$$

$$= \vec{P}_{2+}^{(2)}(t) + \vec{P}_{2-}^{(2)}(t) \tag{3-6}$$

For SFG, we can rewrite $P_1^{(2)}(t)$ as follows:

$$\vec{P}_1^{(2)}(t)_{\mathrm{SFG}} = \vec{P}_{1-}^{(2)}(t)_{\mathrm{SFG}} =$$

$$\vec{P}_{1-}^{(2)}(t)_{\mathrm{SFG}}^{\mathrm{e-e}} + \vec{P}_{1-}^{(2)}(t)_{\mathrm{SFG}}^{\mathrm{e-m}} + \vec{P}_{1-}^{(2)}(t)_{\mathrm{SFG}}^{\mathrm{m-e}} + \vec{P}_{1-}^{(2)}(t)_{\mathrm{SFG}}^{\mathrm{m-m}} \tag{3-7}$$

where $\vec{P}_{1-}^{(2)}(t)_{\mathrm{SFG}}^{\mathrm{e-e}}$, $\vec{P}_{1-}^{(2)}(t)_{\mathrm{SFG}}^{\mathrm{e-m}}$, $\vec{P}_{1-}^{(2)}(t)_{\mathrm{SFG}}^{\mathrm{m-e}}$, and $\vec{P}_{1-}^{(2)}(t)_{\mathrm{SFG}}^{\mathrm{m-m}}$ stand for the electric-dipole−electric-dipole contribution (the e−e mechanism), the electric-dipole−magnetic-dipole contribution (the e−m mechanism), the magnetic-dipole−electric-dipole contribution (the m−e mechanism), and the magnetic-dipole−magnetic-dipole contribution (the m−m mechanism), respectively. $\vec{P}_2^{(2)}(t)_{\mathrm{SFG}}$ can be treated similarly.

As in the linear CD case, we shall show that, for the SFG studies of molecular chirality in solution, we need only to calculate the contributions e−e, e−m, and m−e to $\vec{P}_2^{(2)}(t)$ and the inclusion of the m−m contribution is merely for comparison; it does not have any significant role in our theoretical treatments of the SFG studies of molecular chirality in solution. It is known that the quadrupole contribution is smaller than the magnetic dipole contribution;[37,38] thus, to the order of approximation for contributions e−m and m−e, we shall not consider its effect on the SFG studies of molecular chirality in solution. The SFG expressions for the quadrupole contributions are given in Appendix A.

3.1. Electric-Dipole−Electric-Dipole Contribution. Now we consider $\vec{P}^{(2)}_{1-}(t)^{\mathrm{e-e}}_{\mathrm{SFG}}$ with the energy-ordered states $E_g = \hbar\omega_g < E_k = \hbar\omega_k \equiv E_m < E_{k'} = \hbar\omega_{k'} \equiv E_n$. In this case, we find

$$\vec{P}^{(2)}_{1-}(t)^{\mathrm{e-e}}_{\mathrm{SFG}} = \frac{1}{\hbar^2}\sum_{m,n,g}^{m\neq nk\neq g}\sum_{q\neq p}\exp[-it(\omega_q+\omega_p)]\times \left[\frac{\Delta\sigma_i(gn)\vec{\mu}_{gm}(\hat{V}^{\mathrm{e}}_{q-})_{mn}(\hat{V}^{\mathrm{e}}_{p-})_{ng}}{(\omega'_{mg}-\omega_q-\omega_p)(\omega'_{ng}-\omega_p)} + \frac{\Delta\sigma_i(gm)\vec{\mu}_{gn}(\hat{V}^{\mathrm{e}}_{q-})_{nm}(\hat{V}^{\mathrm{e}}_{p})_{mg}}{(\omega'_{ng}-\omega_q-\omega_p)(\omega'_{mg}-\omega_p)} + \frac{\Delta\sigma_i(ng)\vec{\mu}_{nm}(\hat{V}^{\mathrm{e}}_{q-})_{mg}(\hat{V}^{\mathrm{e}}_{p-})_{gn}}{(\omega'_{mn}-\omega_q-\omega_p)(\omega'_{gn}-\omega_p)} + \frac{\Delta\sigma_i(mg)\vec{\mu}_{mn}(\hat{V}^{\mathrm{e}}_{q-})_{ng}(\hat{V}^{\mathrm{e}}_{p-})_{gm}}{(\omega'_{nm}-\omega_q-\omega_p)(\omega'_{gm}-\omega_p)}\right] \quad (3\text{-}8)$$

Similarly, for $\vec{P}^{(2)}_{2-}(t)^{\mathrm{e-e}}_{\mathrm{SFG}}$, we obtain

$$\vec{P}^{(2)}_{2-}(t)^{\mathrm{e-e}}_{\mathrm{SFG}} = -\frac{1}{\hbar^2}\sum_{m,n,g}^{m\neq n\neq g}\sum_{q\neq p}\exp[-it(\omega_q+\omega_p)]\times \left[\frac{\Delta\sigma_i(gm)\vec{\mu}_{nm}(\hat{V}^{\mathrm{e}}_{q-})_{gn}(\hat{V}^{\mathrm{e}}_{p-})_{mg}}{(\omega'_{mn}-\omega_q-\omega_p)(\omega'_{mg}-\omega_p)} + \frac{\Delta\sigma_i(gn)\vec{\mu}_{mn}(\hat{V}^{\mathrm{e}}_{q-})_{gm}(\hat{V}^{\mathrm{e}}_{p-})_{ng}}{(\omega'_{nm}-\omega_q-\omega_p)(\omega'_{ng}-\omega_p)} + \frac{\Delta\sigma_i(ng)\vec{\mu}_{mg}(\hat{V}^{\mathrm{e}}_{q-})_{nm}(\hat{V}^{\mathrm{e}}_{p-})_{gn}}{(\omega'_{gm}-\omega_q-\omega_p)(\omega'_{gn}-\omega_p)} + \frac{\Delta\sigma_i(kg)\vec{\mu}_{ng}(\hat{V}^{\mathrm{e}}_{q-})_{mn}(\hat{V}^{\mathrm{e}}_{p-})_{gm}}{(\omega'_{gn}-\omega_q-\omega_p)(\omega'_{gm}-\omega_p)}\right] \quad (3\text{-}9)$$

3.2. Electric-Dipole−Magnetic-Dipole Contributions. In a similar fashion, one can compute contributions from electronic and magnetic fields. In this case, we find

$$\vec{P}^{(2)}_{1-}(t)^{\mathrm{e-m}}_{\mathrm{SFG}} = \frac{1}{\hbar^2}\sum_{m,n,g}^{m\neq n\neq g}\sum_{q\neq p}\exp[-it(\omega_q+\omega_p)]\times \left[\frac{\Delta\sigma_i(gn)\vec{\mu}_{gm}(\hat{V}^{\mathrm{e}}_{q-})_{mn}(\hat{V}^{\mathrm{m}}_{p-})_{ng}}{(\omega'_{mg}-\omega_q-\omega_p)(\omega'_{ng}-\omega_p)} + \frac{\Delta\sigma_i(gm)\vec{\mu}_{gn}(\hat{V}^{\mathrm{e}}_{q-})_{nm}(\hat{V}^{\mathrm{m}}_{p-})_{mg}}{(\omega'_{ng}-\omega_q-\omega_p)(\omega'_{mg}-\omega_p)} + \frac{\Delta\sigma_i(ng)\vec{\mu}_{nm}(\hat{V}^{\mathrm{e}}_{q-})_{mg}(\hat{V}^{\mathrm{m}}_{p-})_{gn}}{(\omega'_{mn}-\omega_q-\omega_p)(\omega'_{gn}-\omega_p)} + \frac{\Delta\sigma_i(mg)\vec{\mu}_{mn}(\hat{V}^{\mathrm{e}}_{q-})_{ng}(\hat{V}^{\mathrm{m}}_{p-})_{gm}}{(\omega'_{nm}-\omega_q-\omega_p)(\omega'_{gm}-\omega_p)}\right] \quad (3\text{-}10)$$

and

$$\vec{P}^{(2)}_{1-}(t)^{\mathrm{m-e}}_{\mathrm{SFG}} = \frac{1}{\hbar^2}\sum_{m,n,g}^{m\neq n\neq g}\sum_{q\neq p}\exp[-it(\omega_q+\omega_p)]\times \left[\frac{\Delta\sigma_i(gn)\vec{\mu}_{gm}(\hat{V}^{\mathrm{m}}_{q-})_{mn}(\hat{V}^{\mathrm{e}}_{p-})_{ng}}{(\omega'_{mg}-\omega_q-\omega_p)(\omega'_{ng}-\omega_p)} + \frac{\Delta\sigma_i(gm)\vec{\mu}_{gn}(\hat{V}^{\mathrm{m}}_{q-})_{nm}(\hat{V}^{\mathrm{e}}_{p-})_{mg}}{(\omega'_{ng}-\omega_q-\omega_p)(\omega'_{mg}-\omega_p)} + \frac{\Delta\sigma_i(ng)\vec{\mu}_{nm}(\hat{V}^{\mathrm{m}}_{q-})_{mg}(\hat{V}^{\mathrm{e}}_{p-})_{gn}}{(\omega'_{mn}-\omega_q-\omega_p)(\omega'_{gn}-\omega_p)} + \frac{\Delta\sigma_i(mg)\vec{\mu}_{mn}(\hat{V}^{\mathrm{m}}_{q-})_{ng}(\hat{V}^{\mathrm{e}}_{p-})_{gm}}{(\omega'_{nm}-\omega_q-\omega_p)(\omega'_{gm}-\omega_p)}\right] \quad (3\text{-}11)$$

Note that $\vec{P}^{(2)}_{1-}(t)^{\mathrm{m-m}}_{\mathrm{SFG}}$ can be obtained using $\hat{V}^{\mathrm{m}}_{q-}$ and $\hat{V}^{\mathrm{m}}_{p-}$. $\vec{P}^{(2)}_{2-}(t)_{\mathrm{SFG}}$ can be treated similarly.

In the next several sections, we shall demonstrate the applications of the theoretical results presented in this section.

4. Investigation of Doubly Resonant Infrared−Ultraviolet or Infrared−Visible Sum-Frequency Generation of Chiral Molecules in Solutions

The central problem in SFG is the calculation of the second-order polarization $\vec{P}^{(2)}(t)$ with various polarization combinations. Let $\hat{e}_{S\eta}$ represent the unit vector of the polarization ($\eta = S$ or P) of the sum-frequency radiation, the observed SFG signal is proportional to $|\hat{e}_{S\eta}\cdot\vec{P}^{(2)}_{\eta_1\eta_2}(t)|$,[27,39−41] i.e,

$$I_{\eta\eta_1\eta_2}(t) = \langle|\hat{e}_{S\eta}\cdot\vec{P}^{(2)}_{\eta_1\eta_2}(t)|^2\rangle_{\mathrm{env,ori}} \approx \sum_{l\neq l'}\langle\{\hat{e}_{S\eta}\cdot\vec{P}^{(2)}_{\eta_1\eta_2,l}(t)\}\{\hat{e}_{S\eta}\cdot\vec{P}^{(2)}_{\eta_1\eta_2,l'}(t)\}^*\rangle_{\mathrm{env,ori}} \exp(i\Delta\vec{k}_S\cdot\vec{R}_{ll'}) \quad (4\text{-}1)$$

where $\langle\cdots\rangle_{\mathrm{env,ori}}$ denotes the average over environmental variables and over the orientation of the molecules, and η_1 and η_2 denote the polarizations of the applied fields. If bulk SFG measurements are performed in the $Z-X$ plane (where X and Y denote the laboratory coordinate system and the top and bottom surfaces of the sample are parallel to the X axis).[18,42] The two incident lasers in a noncollinear configuration are focused and overlapped to a spot at the exit surface of the sample.[18] In this case, matching of the wave vector component along the X-direction exists (and no component exists for the Y-directions). However, for the Z-direction, matching of the wave vector component cannot be achieved, because of the limited Z-direction length of the two applied laser fields, whose length should be short enough to avoid the effect of absorption. In this case, the major contribution to the SFG signal results from the molecules in the outermost region of the summation $\Sigma_{l\neq l'}\exp(i\Delta\vec{k}_S\cdot\vec{R}_{ll'})$[40,41] and we can assume that $\vec{P}^{(2)}_{\eta_1\eta_2,l}(t)$ at different sites in such outer regions are not correlated with each other via the environment. This may lead to the factorization

$$\langle\{\hat{e}_{S\eta}\cdot\vec{P}^{(2)}_{\eta_1\eta_2,l}(t)\}\{\hat{e}_{S\eta}\cdot\vec{P}^{(2)}_{\eta_1\eta_2,l'}(t)\}^*\rangle_{\mathrm{env,ori}} = \langle\{\hat{e}_{S\eta}\cdot\vec{P}^{(2)}_{\eta_1\eta_2,l}(t)\}\rangle_{\mathrm{env,ori}}\langle\{\hat{e}_{S\eta}\cdot\vec{P}^{(2)}_{\eta_1\eta_2,l'}(t)\}^*\rangle_{\mathrm{env,ori}} \quad (4\text{-}2)$$

We next assume that, in solution, the molecules are randomly oriented. In this case, we can ignore the subscripts l and l' in eq 4-1, so that we obtain

$$I_{\eta\eta_1\eta_2}(t) \approx \langle S_{\eta\eta_1\eta_2}\rangle_{\mathrm{env,ori}}\langle S^*_{\eta\eta_1\eta_2}\rangle_{\mathrm{env,ori}} \sum_{l\neq l'} \exp(i\Delta\vec{k}_S\cdot\vec{R}_{ll'}) \quad (4\text{-}3)$$

where

$$\langle S_{\eta\eta_1\eta_2}\rangle \equiv \langle\{\hat{e}_{S\eta}\cdot\vec{P}^{(2)}_{\eta_1\eta_2}(t)\}\rangle_{\mathrm{env,ori}} = \langle S^{\mathrm{e-e}}_{\eta\eta_1\eta_2}\rangle + \langle S^{\mathrm{e-m}}_{\eta\eta_1\eta_2}\rangle + \langle S^{\mathrm{m-e}}_{\eta\eta_1\eta_2}\rangle + \langle S^{\mathrm{m-m}}_{\eta\eta_1\eta_2}\rangle \quad (4\text{-}4)$$

and, for example, $\langle S^{\mathrm{e-e}}_{\eta\eta_1\eta_2}\rangle = \langle\{\hat{e}_{S\eta}\cdot\vec{P}^{(2)}_{\eta_1\eta_2}(t)^{\mathrm{e-e}}\}\rangle$.

4.1. Doubly Resonant Sum-Frequency Generation. We shall consider a model for the doubly resonant SFG, in which we assume $E_g = \hbar\omega_g < E_m = \hbar\omega_m < E_n = \hbar\omega_n$ and $\hbar\omega_1 \neq \hbar\omega_2$, as shown in Figure 1A. In this case, we find expressions for environmentally and orientationally averaged $\langle S\rangle$ for the bulk case as

$$\langle S^{\mathrm{e-e}}_{\eta\eta_1\eta_2}\rangle = E_1E_2L(\hat{e}_{S\eta},\hat{e}_{1\eta_1},\hat{e}_{2\eta_2})\sum_g\sum_m\sum_n\Delta\sigma_i(gm)\times \left\{\frac{-[\vec{\mu}_{gn}\cdot(\vec{\mu}_{nm}\times\vec{\mu}_{mg})]}{(\omega_{ng}-i\gamma_{ng}-\omega_1-\omega_2)(\omega_{mg}-i\gamma_{mg}-\omega_1)}\right\}\exp[-it(\omega_1+\omega_2)] \quad (4\text{-}5)$$

and

$$\langle S^{\mathrm{e-m}}_{\eta\eta_1\eta_2}\rangle = \frac{E_1E_2}{c}L(\hat{e}_{S\eta},\hat{e}_{1\eta_1},\hat{b}_{2\eta_2})\sum_g\sum_m\sum_n\Delta\sigma_i(gm)\times \left\{\frac{-[\vec{\mu}_{gn}\cdot(\vec{M}_{nm}\times\vec{\mu}_{mg})]}{(\omega_{ng}-i\gamma_{ng}-\omega_1-\omega_2)(\omega_{mg}-i\gamma_{mg}-\omega_1)}\right\}\exp[-it(\omega_1+\omega_2)] \quad (4\text{-}6)$$

where $E_1 = |\vec{E}^0_1|$ and $E_2 = |\vec{E}^0_2|$, and, for example,

$$L(\hat{e}_{S\eta},\hat{e}_{1\eta_1},\hat{e}_{2\eta_2}) = \frac{\hat{e}_{S\eta}\cdot(\hat{e}_{1\eta_1}\times\hat{e}_{2\eta_2})}{6\hbar^2} \quad (4\text{-}7)$$

The other contributions, $\langle S^{\mathrm{e-e}}_{\eta\eta_1\eta_2}\rangle$ and $\langle S^{\mathrm{e-m}}_{\eta\eta_1\eta_2}\rangle$, can be obtained by proper changes and, thus, hereafter, the expressions for these two terms will not be given.

4.2. Doubly Resonant Infrared−Ultraviolet or Infrared−Visible Sum-Frequency Generation. For the doubly resonant IR−UV SFG of molecules, i.e., $\hbar\omega_1 = \hbar\omega_{\mathrm{IR}}$ and $\hbar\omega_2 = \hbar\omega_{\mathrm{UV}}$, as shown in Figure 1B, we obtain, in the Born−Oppenheimer (B−O) approximation,

$$\langle S^{\mathrm{e-e}}_{\eta\eta_{\mathrm{IR}}\eta_{\mathrm{UV}}}\rangle = E_{\mathrm{IR}}E_{\mathrm{UV}}L(\hat{e}_{S\eta},\hat{e}_{\mathrm{IR}\eta_{\mathrm{IR}}},\hat{e}_{\mathrm{UV}\eta_{\mathrm{UV}}})\sum_v\sum_{v'}\sum_u\Delta\sigma_i(gv,gv')\times \left\{\frac{-[\vec{\mu}_{gv,nu}\cdot(\vec{\mu}_{nu,gv'}\times\vec{\mu}_{gv',gv})]}{(\omega_{nu,gv}-i\gamma_{nu,gv}-\omega_{\mathrm{IR}}-\omega_{\mathrm{UV}})(\omega_{gv',gv}-i\gamma_{gv',gv}-\omega_{\mathrm{IR}})}\right\}\times \exp[-it(\omega_{\mathrm{IR}}+\omega_{\mathrm{UV}})] \quad (4\text{-}8)$$

and

$$\langle S^{\mathrm{e-m}}_{\eta\eta_{\mathrm{IR}}\eta_{\mathrm{UV}}}\rangle = \frac{E_{\mathrm{IR}}E_{\mathrm{UV}}}{c}L(\hat{e}_{S\eta},\hat{e}_{\mathrm{IR}\eta_{\mathrm{IR}}},\hat{b}_{\mathrm{UV}\eta_{\mathrm{UV}}})\sum_v\sum_{v'}\sum_u\Delta\sigma_i(gv,gv')\times \left\{\frac{-[\vec{\mu}_{gv,nu}\cdot(\vec{M}_{nu,gv'}\times\vec{\mu}_{gv',gv})]}{(\omega_{nu,gv}-i\gamma_{nu,gv}-\omega_{\mathrm{IR}}-\omega_{\mathrm{UV}})(\omega_{gv',gv}-i\gamma_{gv',gv}-\omega_{\mathrm{IR}})}\right\}\times \exp[-it(\omega_{\mathrm{IR}}+\omega_{\mathrm{UV}})] \quad (4\text{-}9)$$

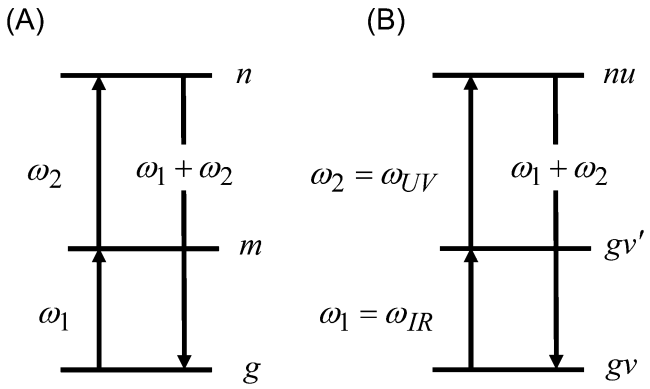

Figure 1. Models for doubly resonant sum-frequency generation (SFG): (A) a general model and (B) a molecular model for doubly resonant infrared−ultraviolet (IR−UV) SFG are shown.

where, for example,

$$\vec{\mu}_{gv',gv} = \langle\Phi_g\Theta_{gv'}|\vec{\mu}|\Phi_g\Theta_{gv}\rangle = \langle\Theta_{gv'}|\vec{\mu}_{gg}|\Theta_{gv}\rangle \quad (4\text{-}10)$$

and

$$\vec{M}_{gv',gv} = \langle\Theta_{gv'}|\vec{M}_{gg}|\Theta_{gv}\rangle \quad (4\text{-}11)$$

etc. Here, $\vec{\mu}_{gg}$ and $\vec{M}_{gg}$ denote the permanent dipole moment and magnetic dipole moment of the ground electronic state g.

Using the Condon approximation (i.e., for allowed electronic transition), we find

$$\vec{\mu}_{gv,nu} = \vec{\mu}_{gn}\langle\Theta_{gv}|\Theta_{nu}\rangle \quad (4\text{-}12)$$

$$\vec{\mu}_{gv',gv} = \sum_l\left(\frac{\partial\vec{\mu}_{gg}}{\partial Q_l}\right)_0\langle\Theta_{gv'}|Q_l|\Theta_{gv}\rangle \quad (4\text{-}13)$$

and

$$\vec{M}_{gv',gv} = \sum_l\left(\frac{\partial\vec{M}_{gg}}{\partial Q_l}\right)_0\langle\Theta_{gv'}|Q_l|\Theta_{gv}\rangle \quad (4\text{-}14)$$

etc. For the system of chiral molecules in solution, $\vec{\mu}_{gn} = \vec{\mu}_{ng}$, so that $\langle S^{\mathrm{e-e}}_{\eta\eta_{\mathrm{IR}}\eta_{\mathrm{UV}}}\rangle = 0$ and if the molecule is not magnetic, then $\vec{M}_{gg} = 0$, so that $\langle S^{\mathrm{m-e}}_{\eta\eta_{\mathrm{IR}}\eta_{\mathrm{UV}}}\rangle = 0$ and $\langle S^{\mathrm{m-m}}_{\eta\eta_{\mathrm{IR}}\eta_{\mathrm{UV}}}\rangle = 0$. In this case, we find

$$\langle S_{\eta\eta_{\mathrm{IR}}\eta_{\mathrm{UV}}}\rangle \equiv \langle\{\hat{e}_{S\eta}\cdot\vec{P}^{(2)}_{\eta_{\mathrm{IR}}\eta_{\mathrm{UV}}}(t)\}\rangle_{\mathrm{env,ori}} = \langle S^{\mathrm{e-m}}_{\eta\eta_{\mathrm{IR}}\eta_{\mathrm{UV}}}\rangle$$

$$= -\frac{E_{\mathrm{IR}}E_{\mathrm{UV}}}{c}L(\hat{e}_{S\eta},\hat{e}_{\mathrm{IR}\eta_{\mathrm{IR}}},\hat{b}_{\mathrm{UV}\eta_{\mathrm{UV}}})\exp[-it(\omega_{\mathrm{IR}}+\omega_{\mathrm{UV}})]\sum_l\left\{\vec{\mu}_{gn}\cdot\left[\vec{M}_{ng}\times\left(\frac{\partial\vec{\mu}_{gg}}{\partial Q_l}\right)_0\right]\right\}\sum_v\sum_{v'}\sum_u \frac{\Delta\sigma_i(gv,gv')}{(\omega_{nu,gv}-i\gamma_{nu,gv}-\omega_{\mathrm{IR}}-\omega_{\mathrm{UV}})(\omega_{gv',gv}-i\gamma_{gv',gv}-\omega_{\mathrm{IR}})} \langle\Theta_{gv}|\Theta_{nu}\rangle\langle\Theta_{nu}|\Theta_{gv'}\rangle\langle\Theta_{gv'}|Q_l|\Theta_{gv}\rangle \quad (4\text{-}15)$$

which should be compared with the SFG of surface molecules in the dipole approximation

$$\langle S_{\eta\eta_{IR}\eta_{UV}}\rangle_{surface} = \langle S^{e-e}_{\eta\eta_{IR}\eta_{UV}}\rangle_{surface} = \frac{E_{IR}E_{UV}}{\hbar^2}\exp[-it(\omega_{IR}+\omega_{UV})]\sum_{v}\sum_{v'}\sum_{u}\Delta\sigma_i(gv,gv')\times \frac{\langle(\vec{\mu}_{gv,nu}\cdot\hat{e}_{S\eta})(\vec{\mu}_{nu,gv'}\cdot\hat{e}_{UV\eta_{UV}})(\vec{\mu}_{gv',gv}\cdot\hat{e}_{IR\eta_{IR}})\rangle_{surface}}{(\omega_{nu,gv}-i\gamma_{nu,gv}-\omega_{IR}-\omega_{UV})(\omega_{gv',gv}-i\gamma_{gv',gv}-\omega_{IR})} \quad (4\text{-}16)$$

or in the Condon approximation

$$\langle S_{\eta\eta_{IR}\eta_{UV}}\rangle_{surface} = \frac{E_{IR}E_{UV}}{\hbar^2}\exp^{-it(\omega_{IR}+\omega_{UV})}\sum_{v}\sum_{v'}\sum_{u}\sum_{l}\frac{\Delta\hat{\sigma}(gv,gv')}{(\omega_{nu,gv}-i\gamma_{nu,gv}-\omega_{IR}-\omega_{UV})(\omega_{gv',gv}-i\gamma_{gv',gv}-\omega_{IR})} \left\langle(\vec{\mu}_{gn}\cdot\hat{e}_{S\eta})(\vec{\mu}_{ng}\cdot\hat{e}_{UV\eta_{UV}})\left[\left(\frac{\partial\vec{\mu}_{gg}}{\partial Q_l}\right)_0\cdot\hat{e}_{IR\eta_{IR}}\right]\right\rangle_{surface} \langle\Theta_{gv}|\Theta_{nu}\rangle\langle\Theta_{nu}|\Theta_{gv'}\rangle\langle\Theta_{gv'}|Q_l|\Theta_{gv}\rangle \quad (4\text{-}17)$$

where $\langle\cdots\rangle_{surface}$ indicates the spatial average performed over the surface. Comparing eq 4-15 with eq 4-17, we can see that the band shapes are the same.

4.3. Non-Condon Scheme. Next, we consider the effect of vibronic coupling on $\langle S^{e-e}_{\eta\eta_{IR}\eta_{UV}}\rangle$ (i.e., beyond the Condon approximation). In this case, the electronic wave function can be expanded in terms of vibronic coordinates Q_p (Appendix B),

$$\vec{\mu}_{ng} = \vec{\mu}^0_{ng} + \sum_p\left(\frac{\partial\vec{\mu}_{ng}}{\partial Q_p}\right)_0 Q_p + \cdots \quad (4\text{-}18)$$

to obtain

$$\langle S^{e-e}_{\eta\eta_{IR}\eta_{UV}}\rangle = E_{IR}E_{UV}L(\hat{e}_{S\eta},\hat{e}_{IR\eta_{IR}},\hat{e}_{UV\eta_{UV}})\exp[-it(\omega_{IR}+\omega_{UV})]\sum_{v}\sum_{v'}\sum_{u}\sum_{p}\sum_{l}\Delta\hat{\sigma}(gv,gv') - \left[\left(\frac{\partial\vec{\mu}_{gn}}{\partial Q_p}\right)_0\cdot\left\{\vec{\mu}^0_{ng}\times\left(\frac{\partial\vec{\mu}_{gg}}{\partial Q_l}\right)_0\right\}\right]\langle\Theta_{gv'}|Q_l|\Theta_{gv}\rangle}{(\omega_{nu,gv}-i\gamma_{nu,gv}-\omega_{IR}-\omega_{UV})(\omega_{gv',gv}-i\gamma_{gv',gv}-\omega_{IR})} [\langle\Theta_{gv}|Q_p|\Theta_{nu}\rangle\langle\Theta_{nu}|\Theta_{gv'}\rangle - \langle\Theta_{gv}|\Theta_{nu}\rangle\langle\Theta_{nu}|Q_p|\Theta_{gv'}\rangle] \quad (4\text{-}19)$$

We can see that the band-shape function is different from that given by eq 4-16 or eq 4-17. From the aforementioned discussion, we can easily see that $\langle S^{e-e}_{\eta\eta_{IR}\eta_{UV}}\rangle_{surface}$ is much larger than $\langle S^{e-e}_{\eta_{IR}\eta_{UV}}\rangle_{surface}$. Comparing eq 4-17 for $\langle S^{e-e}_{\eta_{IR}\eta_{UV}}\rangle_{surface}$ and eq 4-19 for $\langle S^{e-e}_{\eta_{IR}\eta_{UV}}\rangle_{surface}$, we can see that $\vec{\mu}_{gn}$ is involved in the former, whereas $(\partial\vec{\mu}_{gn}/\partial Q_p)_0 Q_p$ is involved in the latter. From Appendix B, we find $(\partial\vec{\mu}_{gn}/\partial Q_p)_0 = \sum_b^{b\neq g}\langle\Phi_b(q,0)|(\partial\hat{H}_e/\partial Q_p)_0|\Phi_g(q,0)\rangle\vec{\mu}^0_{bg}/(U_g(0)-U_b(0))+\cdots$. That is, $\langle S^{e-e}_{\eta\eta_{IR}\eta_{UV}}\rangle$ is 1 order of magnitude smaller than $\langle S^{e-e}_{\eta\eta_{IR}\eta_{UV}}\rangle_{surface}$ by vibronic coupling.

4.4. Breakdown of the Born−Oppenheimer Approximation. The breakdown of the B−O approximation can also be a mechanism that leads to a $\langle S^{e-e}_{\eta\eta_{IR}\eta_{UV}}\rangle$ contribution. The correction of the B−O approximation can be treated as follows:

$$\psi_{nu} = \psi^0_{nu} + \sum_{n'u'}^{n'u'\neq nu}\frac{\langle\psi^0_{n'u'}|\hat{H}'_{BO}|\psi^0_{nu}\rangle}{E_{nu}-E_{n'u'}}\psi^0_{n'u'}+\cdots \quad (4\text{-}20)$$

where ψ^0_{nu} and $\psi^0_{n'u'}$ represent the B−O approximation basis set and

$$\langle\psi^0_{n'u'}|\hat{H}'_{BO}|\psi^0_{nu}\rangle = -\frac{\hbar^2}{2}\sum_p\left\langle\Theta_{n'u'}\left|\left\langle\Phi_{n'}\left|\frac{\partial}{\partial Q_p}\right|\Phi_n\right\rangle\right|\frac{\partial\Theta_{nu}}{\partial Q_p}\right\rangle - \frac{\hbar^2}{2}\sum_p\left\langle\Theta_{n'u'}\left|\left\langle\Phi_{n'}\left|\frac{\partial^2}{\partial Q_p^2}\right|\Phi_n\right\rangle\right|\Theta_{nu}\right\rangle \quad (4\text{-}21)$$

The second term of the right-hand side of eq 4-21 is smaller than the first term and usually neglected. Using eq 4-23, we can obtain

$$\vec{\mu}_{gv,nu} = \vec{\mu}^0_{gv,nu} + \sum_{n'u'}^{n'u'\neq nu}\frac{\langle\psi^0_{n'u'}|\hat{H}'_{BO}|\psi^0_{nu}\rangle}{E_{nu}-E_{n'u'}}\vec{\mu}^0_{gv,n'u'} + \sum_{n''u''}^{n''u''\neq gv}\frac{\langle\psi^0_{n''u''}|\hat{H}'_{BO}|\psi^0_{gv}\rangle}{E_{gv}-E_{n''u''}}\vec{\mu}^0_{n''u'',nu} \quad (4\text{-}22)$$

In this case, we also obtain $\langle S^{e-e}_{\eta\eta_{IR}\eta_{UV}}\rangle \neq 0$ and find that the band-shape function is different from the aforementioned two cases. The contribution from $\hat{H}'_{BO}$ is usually smaller than that from the vibronic coupling (Appendix B). Notice that

$$\vec{\mu}_{gv,nu}\times\vec{\mu}_{nu,gv'} \approx \sum_{n'u'}^{n'u'\neq nu}\frac{\langle\psi^0_{n'u'}|\hat{H}'_{BO}|\psi^0_{nu}\rangle}{E_{nu}-E_{n'u'}}(\vec{\mu}^0_{gv,n'u'}\times\vec{\mu}^0_{nu,gv'} + \vec{\mu}^0_{gv,nu}\times\vec{\mu}^0_{n'u',gv'}) \approx \sum_{n'u'}^{n'u'\neq nu}\frac{\langle\psi^0_{n'u'}|\hat{H}'_{BO}|\psi^0_{nu}\rangle}{E_{nu}-E_{n'u'}}(\vec{\mu}^0_{gn'}\times\vec{\mu}_{ng}{}^0)[\langle\Theta_{gv}|\Theta_{n'u'}\rangle\langle\Theta_{nu}|\Theta_{gv'}\rangle - \langle\Theta_{gv}|\Theta_{nu}\rangle\langle\Theta_{n'u'}|\Theta_{gv'}\rangle] \quad (4\text{-}23)$$

which is nonzero. Here, the contribution from the term $\langle\psi^0_{n''u''}|\hat{H}'_{BO}|\psi^0_{gv}\rangle$ is neglected for simplicity.

4.5. Band-Shape Function. Let us first consider the single-mode case of eq 4-19, i.e., $Q_l = Q_p$. Notice that

$$[\langle\chi_{gv}|Q_p|\chi_{nu}\rangle\langle\chi_{nu}|\chi_{gv'}\rangle - \langle\chi_{gv}|\chi_{nu}\rangle\langle\chi_{nu}|Q_p|\chi_{gv'}\rangle] = \left[\sqrt{\frac{v+1}{2\beta_p}}\langle\chi_{gv+1}|\chi_{nu}\rangle + \sqrt{\frac{v}{2\beta_p}}\langle\chi_{gv-1}|\chi_{nu}\rangle\right]\langle\chi_{nu}|\chi_{gv+1}\rangle - \langle\chi_{gv}|\chi_{nu}\rangle\left[\sqrt{\frac{v+2}{2\beta_p}}\langle\chi_{gu}|\chi_{gv+2}\rangle + \sqrt{\frac{v+1}{2\beta_p}}\langle\chi_{nu}|\chi_{gv}\rangle\right] \quad (4\text{-}24)$$

For $kT \ll \hbar\omega$, we find that eq 4-24 becomes

$$\sqrt{\frac{1}{2\beta_p}}[|\langle\chi_{g1}|\chi_{nu}\rangle|^2 - \sqrt{2}\langle\chi_{g0}|\chi_{nu}\rangle\langle\chi_{nu}|\chi_{g2}\rangle - |\langle\chi_{g0}|\chi_{nu}\rangle|^2] \quad (4\text{-}25)$$

which is not zero, even for the displaced harmonic potential surface case. For the multimode case and $Q_p \neq Q_l$, we find that

$$[\langle\Theta_{gv}|Q_p|\Theta_{nu}\rangle\langle\Theta_{nu}|\Theta_{gv'}\rangle - \langle\Theta_{gv}|\Theta_{nu}\rangle\langle\Theta_{nu}|Q_l|\Theta_{gv'}\rangle] = 0 \quad (4\text{-}26)$$

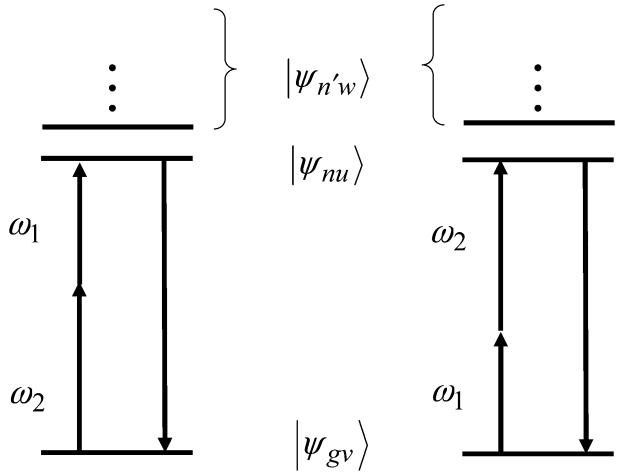

Figure 2. Molecular model of electronically singly resonant SFG of 1,1′-bi-2-naphthol (BN) in the Born−Oppenheimer (B−O) approximation.

whereas for $Q_p = Q_l$,

$$[\langle\Theta_{gv}|Q_p|\Theta_{nu}\rangle\langle\Theta_{nu}|\Theta_{gv'}\rangle - \langle\Theta_{gv}|\Theta_{nu}\rangle\langle\Theta_{nu}|Q_p|\Theta_{gv'}\rangle] \neq 0 \quad (4\text{-}27)$$

The detailed discussion of the band-shape function is presented in Appendix C.

5. SFG in Chiral Liquids near Electronic Resonance

Figure 2 shows a molecular model within the B−O adiabatic approximation for the singly electronic resonant SFG. In this model, the two laser fields (ω_1 and ω_2) are applied to the molecular system and $|\psi_{gv}\rangle = |\Phi_g\rangle|\Theta_{gv}\rangle$, $|\psi_{nu}\rangle = |\Phi_n\rangle|\Theta_{nu}\rangle$, $|\psi_{n'w}\rangle = |\Phi_{n'}\rangle|\Theta_{n'w}\rangle$, where $|\Phi_g\rangle$, $|\Phi_n\rangle$, and $|\Phi_{n'}\rangle$ represent the electronic ground state, the electronic excited-state resonant to the two laser fields, and the electronic off-resonant states, respectively. The corresponding vibrational states are denoted by, for example, $|\Theta_{gv}\rangle$, which represents a multimode vibrational wave function.

In the Condon approximation, we find[24]

$$\langle S^{e-e}_{\eta\eta_1\eta_2}(t)\rangle = \exp[-it(\omega_1+\omega_2)]E_1E_2L(\hat{e}_{S\eta},\hat{e}_{1\eta_1},\hat{e}_{2\eta_2}) \times A^{e-e}(\omega_1,\omega_2,N)F_{ng}(\omega_1+\omega_2) \quad (5\text{-}1)$$

and

$$\langle S^{e-m}_{\eta\eta_1\eta_2}(t)\rangle = \exp[-it(\omega_1+\omega_2)]\frac{E_1E_2}{c}L(\hat{e}_{S\eta},\hat{e}_{1\eta_1},\hat{b}_{2\eta_2}) \times A^{e-m}(\omega_1,\omega_2,N)F_{ng}(\omega_1+\omega_2) \quad (5\text{-}2)$$

where, for example,

$$F_{ng}(\omega_1+\omega_2) \equiv \sum_v\sum_u \frac{\sigma(gv)}{\omega_1+\omega_2-\omega_{nu,gv}+i\gamma_{nu,gv}} \times |\langle\Theta_{nu}|\Theta_{gv}\rangle|^2 \quad (5\text{-}3)$$

$$A^{e-e}(\omega_1,\omega_2,N) = \sum_{n'}^{N}\{\vec{\mu}_{gn}\cdot(\vec{\mu}_{nn'}\times\vec{\mu}_{n'g})\} \times \left[\frac{1}{\omega_2-\omega_{n'g}}-\frac{1}{\omega_1-\omega_{n'g}}\right] \quad (5\text{-}4)$$

and

$$A^{e-m}(\omega_1,\omega_2,N) = \sum_{n'}^{N}\left[\frac{\vec{\mu}_{gn}\cdot(\vec{\mu}_{nn'}\times\vec{M}_{n'g})}{\omega_2-\omega_{n'g}} - \frac{\vec{\mu}_{gn}\cdot(\vec{M}_{nn'}\times\vec{\mu}_{n'g})}{\omega_1-\omega_{n'g}}\right] \quad (5\text{-}5)$$

Note that, in the Condon approximation, the e−e, e−m, m−e, and m−m contributions have the same band-shape function, $F_{ng}(\omega_1+\omega_2)$, and that $A^{e-e}(\omega_1,\omega_2,N)$, $A^{e-m}(\omega_1,\omega_2,N)$, $A^{m-e}(\omega_1,\omega_2,N)$, and $A^{m-m}(\omega_1,\omega_2,N)$ determine the strengths of different SFG mechanisms. $F_{ng}(\omega_1+\omega_2)$ is the same as the band-shape function of the ordinary absorption spectra with $\omega = \omega_1+\omega_2$.

Equations 5-1−5-5 show that the SFG contribution from each mechanism is determined by three factors: (a) laser polarizations and detection alignment conditions (eq 4-9), (b) the band-shape function (eq 5-3), and (c) virtual state contributions (eqs 5-4 and 5-5). Among these factors, condition (c) involves only the electronic transition-dipole moments and/or magnetic transition-dipole moments of the system, and, thus, this factor is dependent on its molecular symmetry and molecular properties.

To calculate factor (c), one can use quantum chemistry methods at various levels. Because BN is quite a large molecule, such quantum chemistry calculation at a high level cannot be practical using our present computational resources. Hence, we first perform a full geometry optimization of BN with hybrid DFT at the B3LYP/6-31G* level.[43] For the electronic and magnetic transition-dipole moment calculations, one can use configuration interaction singles (CIS) or semiempirical methods such as ZINDO/S for the fully optimized geometry.[19,22,23,44] For the sake of simplicity and saving computational time, we shall use the ZINDO/S method for this purpose.

The molecular symmetry should have an important role in SFG/SHG processes of chiral molecules in a solution. To understand how the symmetry affects factor (c), we first investigate BN. Fully optimized structures are found for *S*-BN and *R*-BN molecules with density functional theory (DFT) at the B3LYP/6-31G* level using the Gaussian 03 package.[45] The fully optimized structures exhibit the C_2 symmetry. Some isomers with C_1 symmetry are also found; however, their energies are higher than those of the C_2 symmetry and the transition states are located higher than 1000 cm^{-1}. At room temperature, these other geometries with lower symmetry can well be ignored.

Based on the optimized C_2 symmetry structures, we calculate the electronic transition-dipole moments, the magnetic transition-dipole moments, and the electronic transition energies between any two states within the first 100 singlet states of *S*-BN and *R*-BN. Before proceeding, we first investigate the e−e mechanism. By defining

$$D^{e-e}(n') \equiv \vec{\mu}_{gn}\cdot(\vec{\mu}_{nn'}\times\vec{\mu}_{n'g}) \quad (5\text{-}6)$$

and

$$C(\omega_1,\omega_2,n') \equiv \left[\frac{1}{\omega_2-\omega_{n'g}}-\frac{1}{\omega_1-\omega_{n'g}}\right] \quad (5\text{-}7)$$

eq 5-4 can be rewritten as

$$A^{e-e}(\omega_1,\omega_2,N) \equiv \sum_{n'}^{N}B(\omega_1,\omega_2,n') \equiv \sum_{n'}^{N}D^{e-e}(n')C(\omega_1,\omega_2,n') \quad (5\text{-}8)$$

We compute $D^{e-e}(n')$ and $C(\omega_1,\omega_2,n')$ as a function of the

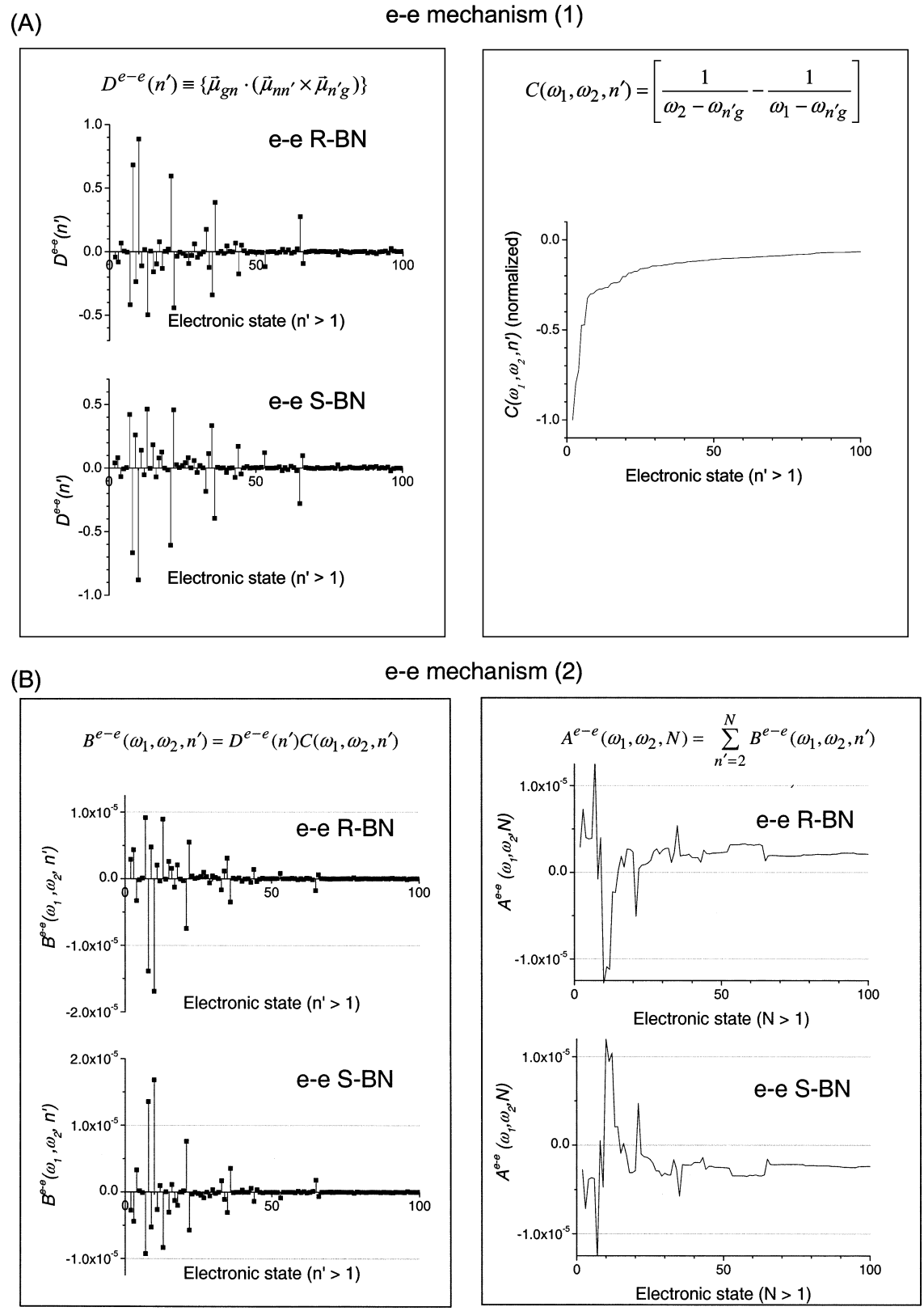

Figure 3. Computed results for the e−e mechanism. Right-hand and left-hand sides of panel A show the calculated $M^{e-e}(n')$ and $C(\omega_1,\omega_2,n')$, respectively. The definitions of these terms are given in the text. These terms are calculated using ZINDO/S for the fully optimized geometries of *R*-BN and *S*-BN. Right-hand and left-hand sides of panel B present the calculated $B^{e-e}(\omega_1,\omega_2,n') = M^{e-e}(n')C(\omega_1,\omega_2,n')$ and $A^{e-e}(\omega_1,\omega_2,N) = \Sigma_{n'=2}^{N} B^{e-e}(\omega_1,\omega_2,n')$, respectively. For the calculation of $A^{e-e}(\omega_1,\omega_2,N)$ and $B^{e-e}(\omega_1,\omega_2,N)$, we adopt values of $\hbar\omega_1 = 9400$ cm^{-1}, $\hbar\omega_2 = 21\,700$ cm^{-1}, and $\hbar\omega_{ng} = 29\,704$ cm^{-1}.[18] In each panel, the upper and lower plots correspond to *R*-BN and *S*-BN, respectively. $M^{e-e}(n')$ values are plotted in atomic units.

electronic excited state n'. For simulation, we adopt $\hbar\omega_1 = 9400$ cm^{-1}, $\hbar\omega_2 = 21\,700$ cm^{-1} and $\hbar\omega_{ng} = 29\,704$ cm^{-1} from ref 18. Right- and left-hand sides of panel A in Figure 3 show the calculated $D^{e-e}(n')$ and $C(\omega_1,\omega_2,n')$, respectively. From panel A, one can see that, to obtain a good convergence, the calculation should be performed at least up to $n' \approx 75$. On the

TABLE 1: Some of the Calculated Electronic Transition-Dipole Moments of *R*-BN[a]

$g \leftrightarrow n$			
μ_x	μ_y	μ_z	λ (nm)
0.2464	−1.1835	0.0000	332.28

	$n \leftrightarrow n'$			$g \leftrightarrow n'$			
state, n'	μ_x	μ_y	μ_z	μ_x	μ_y	μ_z	λ (nm)
1	−0.0693	−0.3847	0.0000	0.0000	0.0000	0.2435	329.29
2	0.0000	0.0000	−0.0914	−1.0305	1.3635	0.0000	314.01
3	0.0493	0.2098	0.0000	0.0000	0.0000	0.6061	307.47
4	0.0317	0.0934	0.0000	0.0000	0.0000	0.0819	277.25
5	0.0000	0.0000	0.0191	0.1073	0.1064	0.0000	277.13
6	0.0000	0.0000	0.1546	1.7516	2.5516	0.0000	249.97
7	0.0000	0.0000	0.3327	−1.5437	−0.9000	0.0000	244.59
8	−0.0199	−0.2041	0.0000	0.0000	0.0000	3.1893	244.04
9	−0.5611	−0.0495	0.0000	0.0000	0.0000	−1.3100	240.04
10	0.0000	0.0000	−0.0844	−1.2192	0.5191	0.0000	237.78
20	0.0000	0.0000	1.0839	−0.5555	0.4394	0.0000	210.59
30	0.1651	0.1006	0.0000	0.0000	0.0000	−0.0928	194.01
40	0.0000	0.0000	−0.0868	0.0130	0.0797	0.0000	182.73
50	−0.0638	0.0715	0.0000	0.0000	0.0000	0.0587	174.73
60	0.0000	0.0000	−0.1149	0.1416	−0.1919	0.0000	169.67
70	0.0000	0.0000	0.0176	0.0375	0.1588	0.0000	163.72
80	−0.1805	−0.0567	0.0000	0.0000	0.0000	0.0058	157.18
90	0.0000	0.0000	−0.0308	−0.4355	−0.0139	0.0000	149.72
100	0.0000	0.0000	0.0555	−0.0645	−0.1688	0.0000	145.42

[a] BN denotes 1,1′-bi-2-naphthol (BN). These matrix elements of the transition-dipole moments are calculated in the molecular coordinates shown in Supporting Information and are given in atomic units. Note that n represents the first electronic excited state and n' denotes other electronic excited states, starting from the second electronic excited state ($n' = 1$).

other hand, the difference of the energy levels $E_{n'+1} - E_{n'}$ for $n' = 1-99$ decreases almost linearly from 10% within $n' < 10$ to ∼1% at $n' \approx 50$ and it becomes almost steady (<1%) for $n' > 50$.

The right- and left-hand sides of panel B in Figure 3 describe the simulation of $B(\omega_1,\omega_2,n')$ and $A^{e-e}(\omega_1,\omega_2,N)$, as a function of the electronic excited state, and that for the summation in eq 5-8, respectively. One can see from the right-hand side of panel B that $B(\omega_1,\omega_2,n')$ converges at $n' \approx 70$. This is due to the slow convergence of $D^{e-e}(n')$ and slow decreasing of $C(\omega_1,\omega_2,n')$, as mentioned previously. From the left-hand side of panel B, one can also see that a good convergence is obtained if the summation is taken up to $N \approx 70$.

From the aforementioned results, we find that, to obtain good converged results, almost 100 excited states should be calculated and included in the SFG calculations at the ZINDO/S level. We should note that $D^{e-e}(n') = \vec{\mu}_{gn} \cdot (\vec{\mu}_{nn'} \times \vec{\mu}_{n'g})$ exhibits a slow convergence behavior. This is due to the fact that this molecule exhibits the twisted conjugated molecular geometry and an oscillatory behavior of transition-dipole moments appears in the z-direction and the $x-y$ plane of the molecular coordinate. Table 1 lists some of the calculated electronic transition-dipole moments of *R*-BN. Our calculation shows that $A^{e-e}(\omega_1,\omega_2,N)$ for *S*-BN and *R*-BN shows different signs.

We have also studied the e−m, m−e, and m−m mechanisms as well and found that the convergence of $\{\vec{\mu}_{gn} \cdot (\vec{M}_{nn'} \times \vec{M}_{n'g})\}$ is slower than that of the e−e mechanism. $A^{m-m}(\omega_1,\omega_2,N)$ also shows different signs for *S*-BN and *R*-BN. Thus, the e−e and m−m mechanisms provide chiral elements that are different for different enantiomers.[18] For the e−m and m−e mechanisms, the transition-dipole moment factors show the same sign for both *S*-BN and *R*-BN. As a result, for these mechanisms, there is no difference between *S*-BN and *R*-BN. In this case,

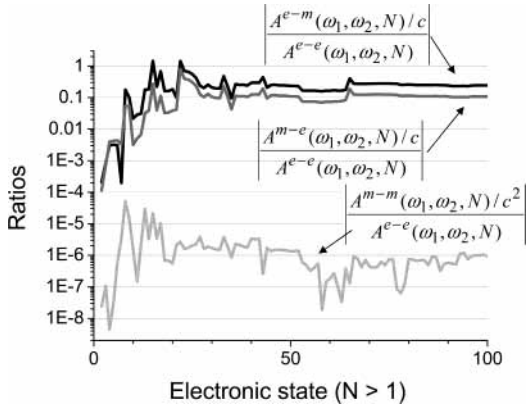

Figure 4. Comparison of the e−e, e−m, and m−e, m−m mechanisms. The ratios of the e−e mechanism to the e−m and m−e mechanisms of BN are determined to be ∼1:0.1, whereas that to the m−m mechanism is ∼$1:10^{-6}$.

$\langle S^{e-m}_{\eta\eta_1\eta_2}(t)\rangle$, $\langle S^{m-e}_{\eta\eta_1\eta_2}(t)\rangle$, and/or $\langle S^{e-m}_{\eta\eta_1\eta_2}(t) + S^{m-e}_{\eta\eta_1\eta_2}(t)\rangle$ may not be zero for racemic systems if the alignments and polarization conditions of both the applied laser field and the detection of SFG signals are appropriately designed. If one considers an experimental configuration,[18,22,23,42] as mentioned in section 4, a question as to whether $\langle S^{e-m}_{\eta\eta_1\eta_2}(t)\rangle$, $\langle S^{m-e}_{\eta\eta_1\eta_2}(t)\rangle$, and/or $\langle S^{e-m}_{\eta\eta_1\eta_2}(t) + S^{m-e}_{\eta\eta_1\eta_2}(t)\rangle$ is zero or not can be examined by choosing $(\eta,\eta_1,\eta_2) = (S, P, S)$ or (S, S, P) polarization conditions for racemic systems. Quite recently, Fischer et al. have, indeed, reported nonzero SFG signals from chiral BN in THF and the intensity of the observed signals are comparable to those observed from a racemic mixture of BN.[23] They have noted that not only is the e−m and m−e mechanism important, but the electric-quadrupole contribution also might participate in the SFG signals with the (S, P, S) and (S, S, P) combinations.

We next calculate the ratio of

$$R^{e-m/m-e}_{e-e}(\omega_1,\omega_2,N) \equiv \frac{\{A^{e-m}(\omega_1,\omega_2,N) + A^{m-e}(\omega_1,\omega_2,N)\}}{A^{e-e}(\omega_1,\omega_2,N)} \tag{5-9}$$

and that of

$$R^{m-m}_{e-e}(\omega_1,\omega_2,N) \equiv \left|\frac{A^{m-m}(\omega_1,\omega_2,N)/c^2}{A^{e-e}(\omega_1,\omega_2,N)}\right| \tag{5-10}$$

as a function of the upper limit N of the summation. Figure 4 shows the comparison of the calculated ratios. One can see from Figure 4 that $R^{e-m}_{e-e}(\omega_1,\omega_2,N)$ and $R^{e-m}_{e-e}(\omega_1,\omega_2,N)$ are within a difference of one order of magnitude, whereas $R^{m-m}_{e-e}(\omega_1,\omega_2,N)$ is 10^{-6}.

We also perform calculations for various chiral molecules in the literature for comparison. For this purpose, we choose R−C_2H_3OF,[19] R−(+)-C_3H_6O,[19] *R*-limonene,[46] and D-arabinose[18,47,48] and perform full geometry optimization for these molecules at the DFT/B3LPY/6-31G* level. Based on the fully optimized structures of these molecules, we calculate $D^{e-e}(n')$ using ZINDO/S. Note that the obtained structures are all C_1 symmetry. One can see from Figures 5A and 3A that the absolute magnitudes of $D^{e-e}(n')$ for these molecules exhibit a tendency of BN ≫ R−C_2H_3OF > R−(+)-C_3H_6O > *R*-limonene > D-arabinose.

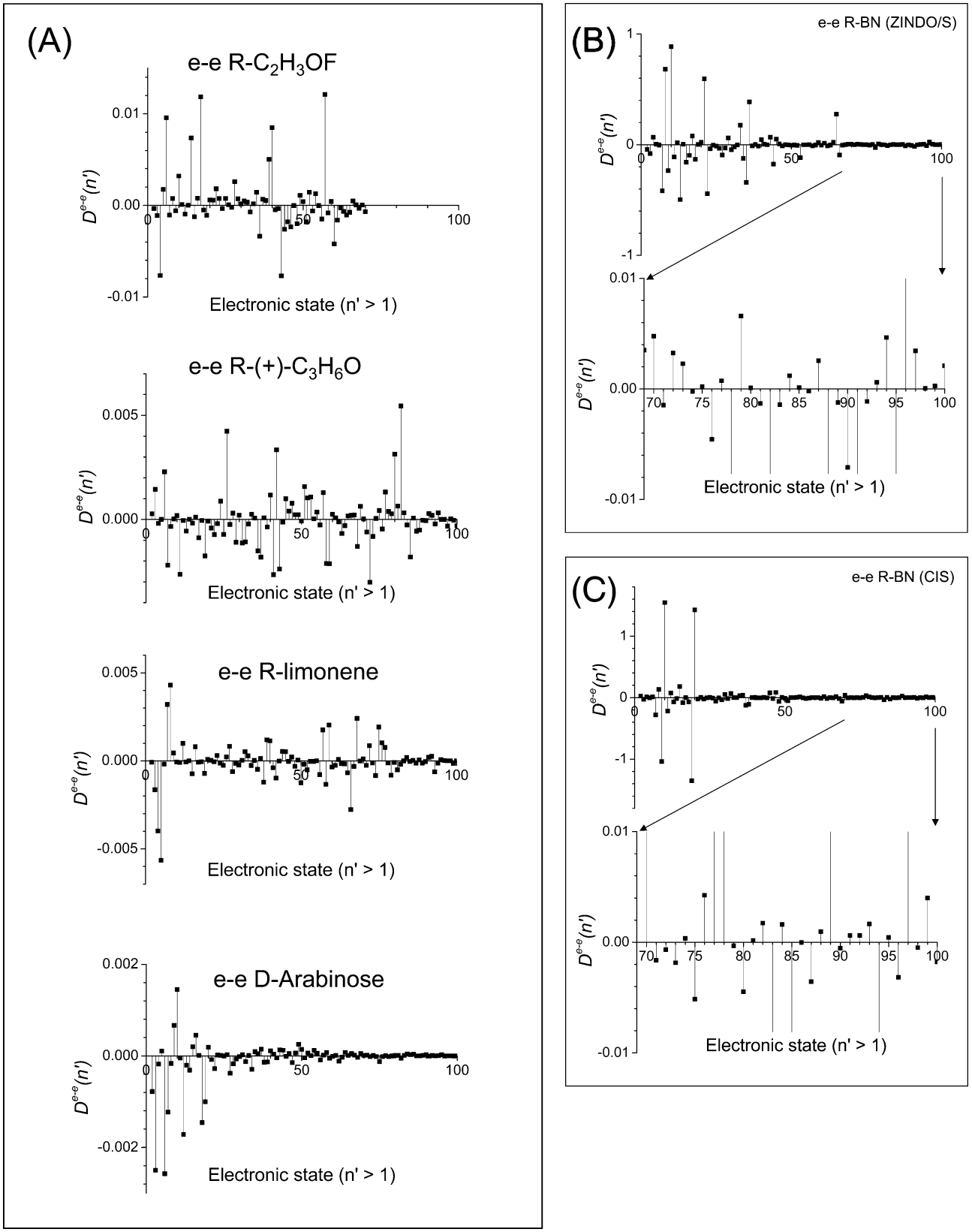

Figure 5. Comparison of the e−e mechanism for various chiral molecules. Panel A shows a comparison of the e−e mechanisms of R−C_2H_3OF, R−(+)-C_3H_6O, *R*-limonene, and D-arabinose, panel B compares ZINDO/S results, and panel C shows CIS results. For panel A, a fully optimized geometry of the electronic ground state of each molecule is obtained using DFT/B3LYP/6-31G* and the optical properties are calculated for the fully optimized geometry using ZINDO/S. The results are plotted in atomic units.

We should note that the chiral SFG response of BN has been calculated by Fischer et al., based on CIS with larger basis sets, and their CIS results indicate that higher substitutions should be included in the configuration interaction.[23] Quinet and Champange[49] have reported the computational results of chiral response of R−C_2H_3OF and R−(+)-C_3H_6O based on the time-

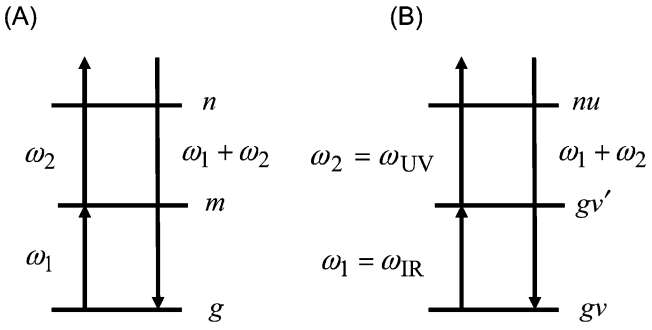

Figure 6. Models for singly resonant SFG: (A) a general model and (B) a molecular model for IR−UV SFG vibrational spectroscopy.

dependent Hartree−Fock method with larger basis sets than those used in this paper. Their results are in close agreement with the SOS/CIS/6-311++G** curves previously reported.[19]

The reasons for the greater electronically resonant SFG response of BN compared with *R*-limonene, D-arabinose, and other molecules can be attributed to the presence of the twisted conjugated molecular geometry of BN and to the relatively large chiral response of BN, which is due to the more-polarizable π-electron system of BN. The twisted conjugated molecular geometry of BN leads to the large triple product of electronic transition-dipole moments involved in SFG.

We also calculate $D^{\mathrm{e-e}}(n') \equiv \vec{\mu}_{gn} \cdot (\vec{\mu}_{nn'} \times \vec{\mu}_{n'g})$ using ab initio at CIS with 6-31G*. The result is shown in Figure 5B and C in atomic units. We obtain a similar behavior of $D^{\mathrm{e-e}}(n')$ as the ZINDO/S calculation for $n' < 25$; however, no distinctive structures are found for $n' > 25$.

Note that the convergence shown in Figures 3−5 only indicates that there are no higher-lying states for a given basis set that can contribute to the summations. Furthermore, it is known that the computation of the magnetic-dipole contribution will be dependent on the choice of the origin of orbitals, unless a complete basis set is used in the computation. To eliminate gauge dependence, the continuous set of gauge transformations (CSGT) and the gauge including/invariant orbitals (GIAO) are implemented in a quantum chemistry calculation package[45] and some of the magnetic properties can be calculated using these methods. In the future, we shall perform the computation with such methods to test the gauge independence of the magnetic-dipole contribution.

Finally, note that a theoretical analysis of real experimental results such as SFG of BN needs molecular modeling to reduce its molecular size and make it possible to perform higher-level quantum chemistry calculations. Quite recently, a quantum coupled-oscillator model for nonlinear optical activity of chiral molecules composed of two coupled monomers in a twisted geometry has been applied to BN with C_2 symmetry.[50]

6. Singly Resonant Sum-Frequency Vibrational Spectroscopy in Chiral Liquids

We shall consider the SFG shown in Figure 6A. Notice that, in this case, we have

$$\vec{P}^{(2)}_{\eta_1\eta_2}(t)^{\mathrm{e-e}} = \frac{1}{\hbar^2}\exp[-it(\omega_1+\omega_2)] \sum_{m,n,g}^{m\neq n\neq g} \frac{\Delta\sigma_i(gm)}{(\omega_{mg}-\omega_1-i\gamma_{mg})} \times \left[\frac{\vec{\mu}_{gn}(\vec{\mu}_{nm}\cdot\vec{E}^0_{2\eta_2})(\vec{\mu}_{mg}\cdot\vec{E}^0_{1\eta_1})}{\omega_{ng}-\omega_1-\omega_2} + \frac{\vec{\mu}_{nm}(\vec{\mu}_{mg}\cdot\vec{E}^0_{1\eta_1})(\vec{\mu}_{gn}\cdot\vec{E}^0_{2\eta_2})}{\omega_{mn}-\omega_1-\omega_2}\right] \quad (6\text{-}1)$$

$$\vec{P}^{(2)}_{\eta_1\eta_2}(t)^{\mathrm{e-m}} = \frac{1}{\hbar^2}\exp[-it(\omega_1+\omega_2)] \sum_{m,n,g}^{m\neq n\neq g} \frac{\Delta\sigma_i(gm)}{(\omega_{mg}-\omega_1-i\gamma_{mg})} \times \left[\frac{\vec{\mu}_{gn}(\vec{M}_{nm}\cdot\vec{B}^0_{2\eta_2})(\vec{\mu}_{mg}\cdot\vec{E}^0_{1\eta_1})}{\omega_{ng}-\omega_1-\omega_2} + \frac{\vec{\mu}_{nm}(\vec{\mu}_{mg}\cdot\vec{E}^0_{1\eta_1})(\vec{M}_{gn}\cdot\vec{B}^0_{2\eta_2})}{\omega'_{mn}-\omega_1-\omega_2}\right] \quad (6\text{-}2)$$

and $\vec{P}^{(2)}_{\eta_1\eta_2}(t)^{\mathrm{m-e}}$ and $\vec{P}^{(2)}_{\eta_1\eta_2}(t)^{\mathrm{m-m}}$ can be obtained easily from eqs 6-1 and 6-2 by proper changes. By taking the spatial average of molecular orientations, we find

$$\langle S^{\mathrm{e-e}}_{\eta\eta_1\eta_2}\rangle = \langle\{\hat{e}_{S\eta}\cdot\vec{P}^{(2)}_{\eta_1\eta_2}(t)^{\mathrm{e-e}}\}\rangle$$

$$= \exp[-it(\omega_1+\omega_2)]E_1E_2L(\hat{e}_{S\eta},\hat{e}_{1\eta_1},\hat{e}_{2\eta_2}) \sum_{m,n,g}^{m\neq n\neq g} \frac{\Delta\sigma_i(gm)}{(\omega_{mg}-\omega_1-i\gamma_{mg})} \times \{\vec{\mu}_{mg}\cdot(\vec{\mu}_{gn}\times\vec{\mu}_{nm})\} \left[\frac{1}{\omega_{mn}-\omega_1-\omega_2} - \frac{1}{\omega_{ng}-\omega_1-\omega_2}\right] \quad (6\text{-}3)$$

and

$$\langle S^{\mathrm{e-m}}_{\eta\eta_1\eta_2}\rangle = \langle\{\hat{e}_{S\eta}\cdot\vec{P}^{(2)}_{\eta_1\eta_2}(t)^{\mathrm{e-m}}\}\rangle =$$

$$\exp[-it(\omega_1+\omega_2)]\frac{E_1E_2}{c}L(\hat{e}_{S\eta},\hat{e}_{1\eta_1},\hat{b}_{2\eta_2}) \times \sum_{m,n,g}^{m\neq n\neq g} \frac{\Delta\sigma_i(gm)}{(\omega_{mg}-\omega_1-i\gamma_{mg})} \left[\frac{\vec{\mu}_{mg}\cdot(\vec{M}_{gn}\times\vec{\mu}_{nm})}{\omega_{mn}-\omega_1-\omega_2} - \frac{\vec{\mu}_{mg}\cdot(\vec{\mu}_{gn}\times\vec{M}_{nm})}{\omega_{ng}-\omega_1-\omega_2}\right] \quad (6\text{-}4)$$

Next, we apply the aforementioned results to IR−UV SFG vibrational spectroscopy, as shown in Figure 6B. In this case, we obtain, in the B−O approximation,

$$\langle S^{\mathrm{e-e}}_{\eta\eta_{\mathrm{IR}}\eta_{\mathrm{UV}}}\rangle = \exp[-it(\omega_{\mathrm{IR}}+\omega_{\mathrm{UV}})]\,E_{\mathrm{IR}}E_{\mathrm{UV}} \times L(\hat{e}_{S\eta},\hat{e}_{\mathrm{IR}\eta_{\mathrm{IR}}},\hat{e}_{\mathrm{UV}\eta_{\mathrm{UV}}}) \sum_{v}\sum_{v'}\sum_{nu} \frac{\Delta\sigma_i(gv,gv')}{\omega_{gv',gv}-\omega_{\mathrm{IR}}-i\gamma_{gv',gv}} \times \{\vec{\mu}_{gv',gv}\cdot(\vec{\mu}_{gv,nu}\times\vec{\mu}_{nu,gv'})\}\left[\frac{1}{\omega_{gv',nu}-\omega_{\mathrm{IR}}-\omega_{\mathrm{UV}}} - \frac{1}{\omega_{nu,gv}-\omega_{\mathrm{IR}}-\omega_{\mathrm{UV}}}\right] \quad (6\text{-}5)$$

and we find

$$\sum_u (\vec{\mu}_{gv,nu} \times \vec{\mu}_{nu,gv'}) = \sum_u \langle \Theta_{gv}|\vec{\mu}_{gn}|\Theta_{nu}\rangle \times \langle \Theta_{nu}|\vec{\mu}_{ng}|\Theta_{gv'}\rangle = \langle \Theta_{gv}|\vec{\mu}_{gn} \times \vec{\mu}_{ng}|\Theta_{gv'}\rangle = 0 \quad (6\text{-}6)$$

because $\vec{\mu}_{gn} \times \vec{\mu}_{ng} = 0$ for low-symmetry molecules.

We shall show that, taking into account the breakdown of the B−O approximation, $\langle S_{e-e}\rangle \neq 0$. Notice that

$$\psi_{nu} = \psi^0_{nu} + \sum_{mw}^{mw\neq nu} \frac{\langle \psi^0_{mw}|\hat{H}'_{BO}|\psi^0_{nu}\rangle}{E_{nu} - E_{mw}} \psi^0_{mw} + \cdots \quad (6\text{-}7)$$

$$\psi_{gv} = \psi^0_{gv} + \sum_{m'w'}^{m'w'\neq gv} \frac{\langle \psi^0_{m'w'}|\hat{H}'_{BO}|\psi^0_{gv}\rangle}{E_{gv} - E_{m'w'}} \psi^0_{gv} + \cdots \quad (6\text{-}8)$$

and

$$\vec{\mu}_{gv,nu} \times \vec{\mu}_{nu,gv'} = \sum_{mw}^{mw\neq nu} \frac{\langle \psi^0_{mw}|\hat{H}'_{BO}|\psi^0_{nu}\rangle}{E_{nu} - E_{mw}} (\vec{\mu}^0_{gv,mw} \times \vec{\mu}^0_{nu,gv'} + \vec{\mu}^0_{gv,nu} \times \vec{\mu}^0_{mw,gv'}) + \sum_{m'w'}^{m'w'\neq gv} \frac{\langle \psi^0_{m'w'}|\hat{H}'_{BO}|\psi^0_{gv}\rangle}{E_{nu} - E_{m'w'}} (\vec{\mu}^0_{m'w',nu} \times \vec{\mu}^0_{nu,gv'}) + \sum_{m''w''}^{m''w''\neq nu} \frac{\langle \psi^0_{m''w''}|\hat{H}'_{BO}|\psi^0_{gv}\rangle}{E_{nu} - E_{m''w''}} (\vec{\mu}^0_{gv,nu} \times \vec{\mu}^0_{nu,m''w''}) + \cdots \quad (6\text{-}9)$$

We can similarly show that the non-Condon effect can also make $\langle S^{e-e}_{\eta\eta_1\eta_2}\rangle \neq 0$.

Next, if we let

$$\vec{T}^{e-e}_{gv,gv'}(nu) = \vec{\mu}_{gv,nu} \times \vec{\mu}_{nu,gv'} \quad (6\text{-}10)$$

then eq 6-5 becomes

$$\langle S^{e-e}_{\eta\eta_{IR}\eta_{UV}}\rangle = \exp[-it(\omega_{IR} + \omega_{UV})]E_1E_2 \times L(\hat{e}_{S\eta},\hat{e}_{IR\eta_{IR}},\hat{e}_{UV\eta_{UV}}) \sum_v \sum_{v'} \sum_{nu} \langle \Theta_{gv}|Q_l|\Theta_{gv'}\rangle \times \frac{\Delta\sigma(gv,gv')\left\{\left(\frac{\partial\vec{\mu}_{gg}}{\partial Q_l}\right)_0 \cdot \vec{T}^{e-e}_{gv,gv'}(nu)\right\}}{\omega_{gv',gv} - \omega_{IR} - i\gamma_{gv',gv}} \frac{-\omega_{ng}}{(\omega_{ng})^2 - (\omega_{IR} + \omega_{UV})^2} \quad (6\text{-}11)$$

Next, we consider $\langle S_{d-m}\rangle$. For diamagnetic molecules, we obtain

$$\langle S^{e-m}_{\eta\eta_{IR}\eta_{UV}}\rangle = \exp[-it(\omega_{IR} + \omega_{UV})]\frac{E_{IR}E_{UV}}{c} \times L(\hat{e}_{S\eta},\hat{e}_{IR\eta_{IR}},\hat{b}_{UV\eta_{UV}}) \sum_v \sum_{v'} \sum_{nu} \frac{\Delta\sigma_i(gv,gv')}{\omega_{gv',gv} - \omega_{IR} - i\gamma_{gv',gv}} \times \vec{\mu}_{gv',gv} \cdot \left[\frac{(\vec{M}_{gv,nu} \times \vec{\mu}_{nu,gv'})}{\omega_{gv',nu} - \omega_{IR} - \omega_{UV}} - \frac{(\vec{\mu}_{gv,nu} \times \vec{M}_{nu,gv'})}{\omega_{nu,gv} - \omega_{IR} - \omega_{UV}}\right] \quad (6\text{-}12)$$

Applying the Placzek approximation (i.e., $\omega_{nu,gv} \approx \omega_{ng}$ and $\omega_{gv,nu} \approx \omega_{gn}$) to eq 6-12 reduces to

$$\langle S^{e-m}_{\eta\eta_{IR}\eta_{UV}}\rangle = \exp[-it(\omega_{IR} + \omega_{UV})]\frac{E_{IR}E_{UV}}{c} \times L(\hat{e}_{S\eta},\hat{e}_{IR\eta_{IR}},\hat{b}_{UV\eta_{UV}}) \sum_v \sum_{v'} \sum_n \sum \frac{\Delta\sigma_i(gv,gv')\langle \Theta_{gv'}|\vec{\mu}_{gg}|\Theta_{gv}\rangle}{\omega_{gv',gv} - \omega_{IR} - i\gamma_{gv',gv}} \cdot \left\langle \Theta_{gv}\left|\left[\frac{(\vec{M}_{gn} \times \vec{\mu}_{ng})}{\omega_{gn} - \omega_{IR} - \omega_{UV}} - \frac{(\vec{\mu}_{gn} \times \vec{M}_{ng})}{\omega_{ng} - \omega_{IR} - \omega_{UV}}\right]\right|\Theta_{gv'}\right\rangle \quad (6\text{-}13)$$

If we define

$$\vec{T}^{e-m}_{gg}(\omega_{IR},\omega_{UV}) = \sum_n \left[\frac{(\vec{M}_{gn} \times \vec{\mu}_{ng})}{\omega_{gn} - \omega_{IR} - \omega_{UV}} - \frac{(\vec{\mu}_{gn} \times \vec{M}_{ng})}{\omega_{ng} - \omega_{IR} - \omega_{UV}}\right] \quad (6\text{-}14)$$

eq 6-13 becomes

$$\langle S^{e-m}_{\eta\eta_{IR}\eta_{UV}}\rangle = \exp[-it(\omega_{IR} + \omega_{UV})]\frac{E_{IR}E_{UV}}{c} \times L(\hat{e}_{S\eta},\hat{e}_{IR\eta_{IR}},\hat{b}_{UV\eta_{UV}}) \sum_v \sum_{v'} \frac{\Delta\sigma_i(gv,gv')}{\omega_{gv',gv} - \omega_{IR} - i\gamma_{gv',gv}} \times \{\langle \Theta_{gv'}|\vec{\mu}_{gg}|\Theta_{gv}\rangle \cdot \langle \Theta_{gv}|\vec{T}^{e-m}_{gg}(\omega_{IR},\omega_{UV})|\Theta_{gv'}\rangle\} \quad (6\text{-}15)$$

or

$$\langle S^{e-m}_{\eta\eta_{IR}\eta_{UV}}\rangle = \exp[-it(\omega_{IR} + \omega_{UV})]\frac{E_{IR}E_{UV}}{c} \times L(\hat{e}_{S\eta},\hat{e}_{IR\eta_{IR}},\hat{b}_{UV\eta_{UV}}) \sum_l \sum_v \sum_{v'} \frac{\Delta\sigma_i(gv,gv')|\langle \Theta_{gv}|Q_l|\Theta_{gv'}\rangle|^2}{\omega_{gv',gv} - \omega_{IR} - i\gamma_{gv',gv}} \times \left\{\left(\frac{\partial\vec{\mu}_{gg}}{\partial Q_l}\right)_0 \cdot \left(\frac{\partial\vec{T}^{e-m}_{gg}(\omega_{IR},\omega_{UV})}{\partial Q_l}\right)_0\right\} \quad (6\text{-}16)$$

Similarly, we have

$$\langle S^{m-e}_{\eta\eta_{IR}\eta_{UV}}\rangle = \exp[-it(\omega_{IR} + \omega_{UV})]\frac{E_{IR}E_{UV}}{c} \times L(\hat{e}_{S\eta},\hat{b}_{IR\eta_{IR}},\hat{e}_{UV\eta_{UV}}) \sum_l \sum_v \sum_{v'} \frac{\Delta\sigma_i(gv,gv')|\langle \Theta_{gv}|Q_l|\Theta_{gv'}\rangle|^2}{\omega_{gv',gv} - \omega_{IR} - i\gamma_{gv',gv}} \times \left\{\left(\frac{\partial\vec{M}_{gg}}{\partial Q_l}\right)_0 \cdot \left(\frac{\partial\vec{T}^{m-e}_{gg}(\omega_{IR},\omega_{UV})}{\partial Q_l}\right)_0\right\} \quad (6\text{-}17)$$

where

$$\vec{T}^{m-e}_{gg}(\omega_{IR},\omega_{UV}) = \sum_n \left[\frac{(\vec{\mu}_{gn} \times \vec{\mu}_{ng})}{\omega_{gn} - \omega_{IR} - \omega_{UV}} - \frac{(\vec{\mu}_{gn} \times \vec{\mu}_{ng})}{\omega_{ng} - \omega_{IR} - \omega_{UV}}\right] = \sum_n (\vec{\mu}_{gn} \times \vec{\mu}_{ng})\left[\frac{-\omega_{ng}}{(\omega_{ng})^2 - (\omega_{IR} + \omega_{UV})^2}\right] \quad (6\text{-}18)$$

which is zero for low-symmetry molecules, and

$$\langle S\eta^{\mathrm{m-m}}_{\eta\eta_{\mathrm{IRUV}}}\rangle = \exp[-it(\omega_{\mathrm{IR}}+\omega_{\mathrm{UV}})]\frac{E_{\mathrm{IR}}E_{\mathrm{UV}}}{c^2}\times L(\hat{e}_{S\eta},\hat{b}_{\mathrm{IR}\eta_{\mathrm{IR}}},\hat{b}_{\mathrm{UV}\eta_{\mathrm{UV}}})\sum_l\sum_v\sum_{v'}\frac{\Delta\sigma_i(gv,gv')|\langle\Theta_{gv}|Q_l|\Theta_{gv'}\rangle|^2}{\omega_{gv',gv}-\omega_{\mathrm{IR}}-i\gamma_{gv',gv}}\times\left(\frac{\partial\vec{M}_{gg}}{\partial Q_l}\right)_0\cdot\left(\frac{\partial\vec{T}^{\mathrm{m-m}}_{gg}}{\partial Q_l}\right)_0 \quad (6\text{-}19)$$

Here, we have

$$\vec{T}^{\mathrm{m-m}}_{gg}(\omega_{\mathrm{IR}},\omega_{\mathrm{UV}}) = \vec{T}^{\mathrm{e-m}}_{gg}(\omega_{\mathrm{IR}},\omega_{\mathrm{UV}}) \quad (6\text{-}20)$$

7. Discussions

Now, we are in a position to apply the theoretical results to the experimentally observed SFG spectra in various cases. For this purpose, we consider three cases: (i) near-electronic resonance SFG, (ii) singly resonant IR−UV SFG, and (iii) doubly resonant IR−UV SFG. We calculate the polarization combinations $L(\hat{e}_{S\eta},\hat{e}_{1\eta_1},\hat{e}_{2\eta_2})$, $L(\hat{e}_{S\eta},\hat{e}_{1\eta_1},\hat{b}_{2\eta_2})$, $L(\hat{e}_{S\eta},\hat{b}_{1\eta_1},\hat{e}_{2\eta_2})$, and $L(\hat{e}_{S\eta},\hat{b}_{1\eta_1},\hat{b}_{2\eta_2})$ for the aforementioned three SFG cases, and the results are listed in Tables 2, 3, and 4, respectively.

In the following, we shall show the importance of the measurements of laser polarizations and SFG band-shape functions in the SFG studies of molecular chirality in solution (e.g., in the determination of chiral and achiral contributions in the SFG experiments).

7.1. Near-Electronic Resonant Sum-Frequency Generation. The transmission SFG spectra of BN in tetrahydrofuran (THF) with (a) SPP and (b) PPS polarization combinations measured by Shen et al.[18] are reproduced in Figure 7. Their experimental geometry (θ_1, θ_2, and θ_S) and the definition of polarizations (*P*-polarization and *S*-polarization) are also depicted in Figure 7. Theoretical treatments of this SFG are given in Section 5. Equations 5-1−5-5 show that the effect of laser polarizations is determined by $L(\hat{e}_{s\eta},\hat{e}_{1\eta_1},\hat{e}_{2\eta_2})$, whereas $A^{\mathrm{e-e}}(\omega_1,\omega_2,N)$ and $A^{\mathrm{e-m}}(\omega_1,\omega_2,N)$ (see eqs 5-4 and 5-5) determine the strength of $\langle S^{\mathrm{e-e}}_{\eta\eta_1\eta_2}(t)\rangle$ and $\langle S^{\mathrm{e-m}}_{\eta\eta_1\eta_2}(t)\rangle$, respectively. Table 2 shows that, for the SPP case, the SFG signal is proportional to $\sin^2(\theta_1+\theta_2)$, whereas, for the PPS case, the SFG signal is proportional to $\sin^2(\theta_1+\theta_S)$. From their experimental geometry, one notices that $\theta_1+\theta_2 = 78° > 34° + \theta_S$, so that the intensity of the SPP case is larger than that of the PPS case. From eqs 5-1−5-5, one can readily see that the band-shape functions for both cases should be the same as those shown by Figure 7 and are given by $F_{ng}(\omega_1+\omega_2)$.

7.2. Singly Resonant Infrared−Ultraviolet Sum-Frequency Generation. The vibrational SFG spectra of limonese in transmission in SPP, PSP (chiral spectra), SSP, SPS, and PPP (achiral spectra) polarization combinations obtained by Shen et al.[46] are shown in Figure 8. Their experimental geometry can be obtained by exchanging ω_1 and θ_1 with ω_2 and θ_2 in Figure 8, and $\theta_1+\theta_2 = 90°$. Here, ω_1 and ω_2 represent infrared and visible laser frequencies, respectively. Table 3 shows that the SFG signal for the SPP case is proportional to $\sin^2(\theta_1+\theta_2)$, whereas that for the PSP case is proportional to $\sin^2(\theta_2-\theta_S)$. From their experimental geometry, one can see that $\theta_1+\theta_2 = 90° > |\theta_2-\theta_S|$. In this case, the intensity of the SPP case is stronger than that of the PPS case. In other words, the intensities of these two cases will be different but their band-shape functions should be the same; this can be seen from panels a and b in Figure 8. Table 3 shows that the three cases SSP, SPS, and PPP can be due to the contributions from the electric-dipole−magnetic-dipole SFG and/or the magnetic-dipole−electric-dipole SFG; thus, their SFG signals will be weaker than those from the electric-dipole−electric-dipole SFG (SPP and PSP).

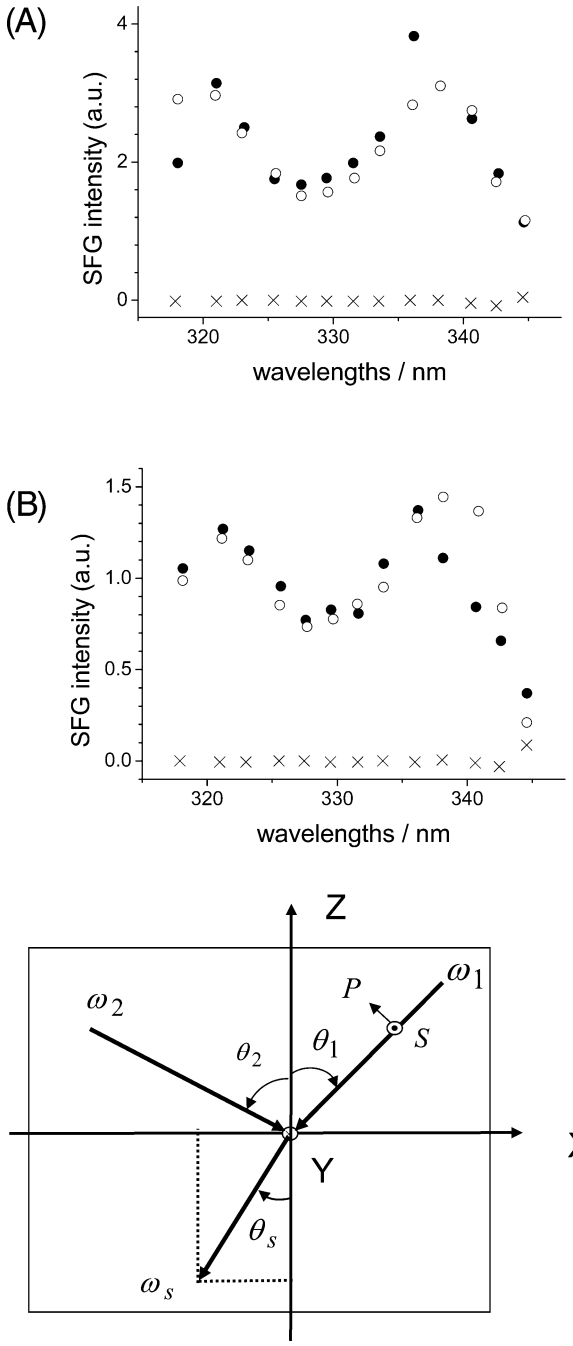

Figure 7. Near-electronic resonance SFG of BN in tetrahydrofuran (THF) solution with (A) SPP and (B) PPS polarization combinations ((●) *S*-BN, (○) *R*-BN, and (×) racemic mixture). Data points are adopted from ref 18.

One can see from Figure 8 that the IR spectral profiles of the singly resonant IR-vis SFG under different polarization combinations are different. In particular, one can notice that there are differences in the relative peak intensities of the different vibrational bands. Equations 6-11, 6-16, and 6-17 show that the selection rules are, in principle, different $((\partial\vec{\mu}_{gg}/\partial Q_l)_0 \neq 0$ and $\vec{T}^{\mathrm{e-e}}_{gv,gv'}(nu) \neq 0$ for e−e, $(\partial\vec{\mu}_{gg}/\partial Q_l)_0 \neq 0$ and $(\partial\vec{T}^{\mathrm{e-m}}_{gg}(\omega_1,\omega_2)/\partial Q_l)_0 \neq 0$ for e−m, and $(\partial M_{gg}/\partial Q_l)_0 \neq 0$ and

TABLE 2: Laser and Detection Polarization Combinations for the Transmission Sum-Frequency Generation (SFG) Spectra of the Near-Electronic Resonance SFG of BN in Tetrahydrofuran (THF)[a]

polarization combination, $\eta\eta_1\eta_2$	e−e $\hat{e}_{S\eta} \cdot (\hat{e}_{1\eta_1} \times \hat{e}_{2\eta_2})$	e−m $\hat{e}_{S\eta} \cdot (\hat{e}_{1\eta_1} \times \hat{b}_{2\eta_2})$	m−e $\hat{e}_{S\eta} \cdot (\hat{b}_{1\eta_1} \times \hat{e}_{2\eta_2})$	m−m $\hat{e}_{S\eta} \cdot (\hat{b}_{1\eta_1} \times \hat{b}_{2\eta_2})$
PPP	0	$\sin(\theta_1 + \theta_S)$	$\sin(\theta_2 - \theta_S)$	0
SSS	0	0	0	$\sin(\theta_1 + \theta_2)$
SPS	0	$\sin(\theta_1 + \theta_2)$	0	0
PSS	0	$\sin(\theta_2 - \theta_S)$	$\sin(\theta_1 + \theta_S)$	0
SSP	0	0	$-\sin(\theta_1 + \theta_2)$	0
SPP	$-\sin(\theta_1 + \theta_2)$	0	0	0
PPS	$\sin(\theta_1 + \theta_S)$	0	0	$-\sin(\theta_2 - \theta_S)$
PSP	$-\sin(\theta_2 - \theta_S)$	0	0	$\sin(\theta_1 + \theta_2)$

[a] Experimental geometry from ref 18 is used.

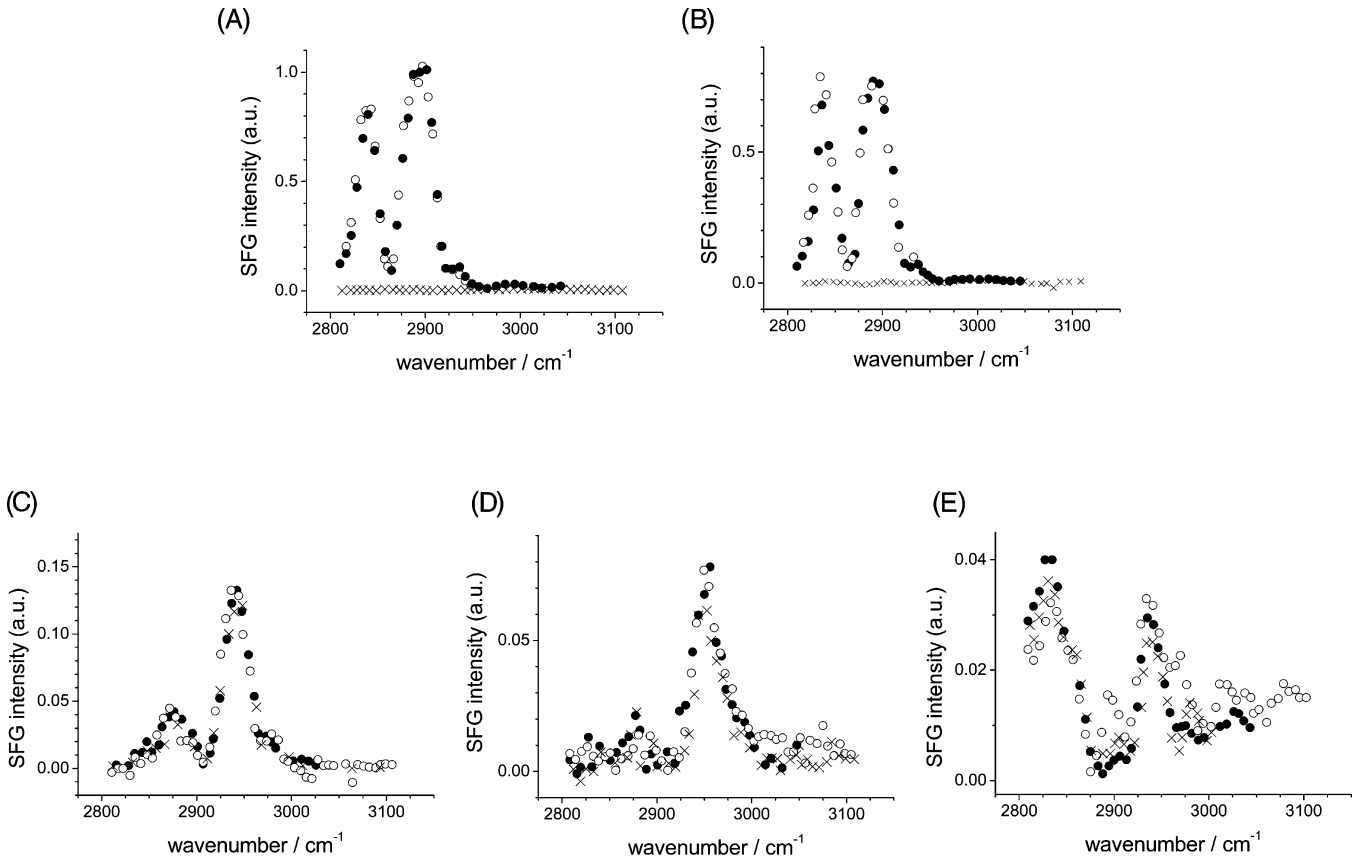

Figure 8. Singly resonant IR−UV SFG of limonene in solution. Various polarization combinations are shown for (A) SPP, (B) PSP, (C) PPP, (D) SSP, and (E) SPS ((●) *S*-limonene, (○) *R*-limonene, and (×) racemic mixture). Data points are adopted from ref 46.

TABLE 3: Laser and Detection Polarization Combinations for the Singly Resonant IR−UV SFG Spectra of Limonese in Transmission[a]

polarization combination, $\eta\eta_1\eta_2$	e−e $e_{S\eta} \cdot (\hat{e}_{1\eta_1} \times \hat{e}_{2\eta_2})$	e−m $\hat{e}_{S\eta} \cdot (\hat{e}_{1\eta_1} \times \hat{b}_{2\eta_2})$	m−e $\hat{e}_{S\eta} \cdot (\hat{b}_{1\eta_1} \times \hat{e}_{2\eta_2})$	m−m $\hat{e}_{S\eta} \cdot (\hat{b}_{1\eta_1} \times \hat{b}_{2\eta_2})$
PPP	0	$\sin(\theta_1 + \theta_S)$	$\sin(\theta_2 - \theta_S)$	0
SSS	0	0	0	$-\sin(\theta_1 + \theta_2)$
SPS	0	$\sin(\theta_1 + \theta_2)$	0	0
PSS	0	$\sin(\theta_2 - \theta_S)$	$\sin(\theta_1 + \theta_S)$	0
SSP	0	0	$-\sin(\theta_1 + \theta_2)$	0
SPP	$\sin(\theta_1 + \theta_2)$	0	0	0
PPS	$-\sin(\theta_1 + \theta_S)$	0	0	$\sin(\theta_2 - \theta_S)$
PSP	$\sin(\theta_2 - \theta_S)$	0	0	$-\sin(\theta_1 + \theta_S)$

[a] Experimental geometry from ref 46 is used.

$(\partial \vec{T}_{gg}^{m-e}(\omega_1,\omega_2)/\partial Q_l)_0 \neq 0$ for m−e). This implies that the observed difference in the relative peak intensities of the different vibrational bands for various polarization combinations is partially due to the selection rules.

7.3. Doubly Resonant Infrared−Ultraviolet Sum-Frequency Generation. The IR−SFG (SPP) spectrum of the *R*-BN in acetone solution and the IR−SFG (SSP) spectrum of the monolayer of *R*-BN in water obtained by Shen et al.[51] are shown in Figure 9, as a function of ω_{IR}. Their experimental geometry (θ_1, θ_2, and θ_S) is also depicted in Figure 9. These data points are adopted from the experimental results measured at $\lambda_{UV} =$ 335 nm, which is near the location of the first absorption peak.

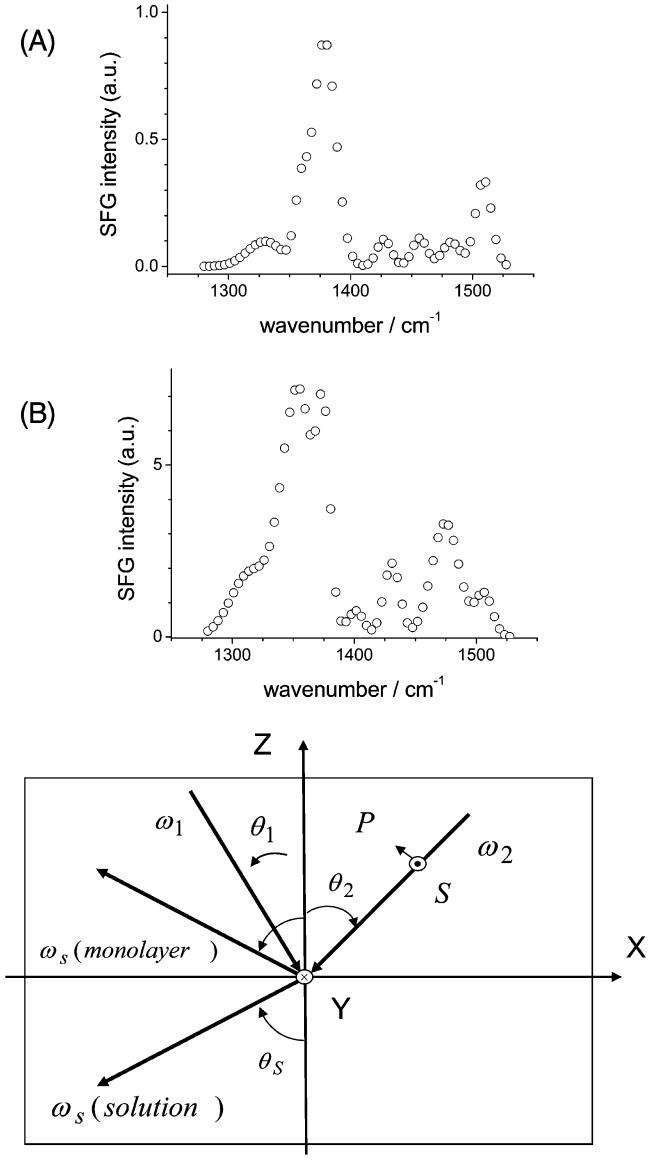

Figure 9. Doubly resonant IR−UV SFG of *R*-BN. Panels A and B are for *R*-BN in acetone solution and an *R*-BN monolayer on water, respectively. Data points are adopted from the $\lambda_{UV} = 335$ nm case given in ref 51.

$\langle S^{e-e}_{\eta\eta_{IR}\eta_{UV}}\rangle$ and $\langle S^{e-e}_{\eta\eta_{IR}\eta_{UV}}\rangle_{surface}$ are given by eqs 4-8 and 4-16, which contain the information of the polarization dependence and the band-shape functions. Table 4 shows that the laser and detection polarization combinations are related to the solution experimental geometry. The SFG intensity difference in solution and on surface is due to the fact that the former is zero in the electric-dipole−electric-dipole approximation (eq 4-8) within the Condon approximation), and the effect of either the non-Condon effect (eq 4-19) or the breakdown of the B−O approximation (eq 4-23) must be included to make the SFG nonzero. Note that $\langle S^{e-e}_{\eta\eta_{IR}\eta_{UV}}\rangle$ can also become allowed by including the magnetic dipole contribution, that is $\langle S^{e-m}_{\eta\eta_{IR}\eta_{UV}}\rangle$ and/or $\langle S^{m-e}_{\eta\eta_{IR}\eta_{UV}}\rangle$. According to our theoretical results, we expect that the band shapes for these figures should be different, as shown in Figure 9.

In this paper, band-shape functions of various SFG spectra have only been discussed qualitatively, because the quantitative calculations of these band-shape functions are usually quite complicated. A detailed calculation of the band-shape function of doubly resonant IR−UV SFG has been presented in a previous paper.[25] In Appendix C, the calculation of band-shape functions of the doubly resonant IR−UV SFG induced by the non-Condon effect is presented.

Three different types of SFG—near-electronic resonant vis-vis SFG, singly resonant IR−UV SFG, and doubly resonant IR−UV SFG—have been treated in this paper. These SFG spectra generally can be separated into the band-shape function and the term that involves electronic matrix elements. For the near-electronic resonant vis-vis SFG, it is allowed in the electric-dipole−dipole approximation; thus, the electronic matrix elements involved in this SFG can be calculated in a straightforward manner. For the other two SFGs, they are forbidden in the electric-dipole−dipole approximation; therefore, in addition to taking into account the magnetic-dipole contribution, it is necessary to include the calculation of vibronic couplings in the calculation of original electronic-matrix elements. The contribution of vibronic coupling to these two SFGs can originate from the non-Condon effect and the effect of the breakdown of the B−O approximation. Quantitative discussion of these two types of SFG will be reported in the future.

Note that the SFG expressions presented in this paper are, in the exact sense, applicable only for homogeneously broadened peaks. The existence of inhomogeneities in the liquid or on the surface can introduce additional broadening. This inhomogeneous effect has been treated in our previous paper.[25] A brief discussion is given in Appendix C.

In summary, we have derived theoretical expressions for SFG signals which can be applied to study various SFG experiments. As applications, we have discussed, in detail, the SFG treatments for the near-electronic resonant, singly resonant IR−UV, and doubly resonant IR−UV cases that are associated with the measurements reported by Shen's group. In particular, we have taken into account both the electric- and magnetic-dipole interactions and the applied laser and detection polarization combinations explicitly. Based on the molecular−theoretical expressions for SFG, we have clarified how polarization combinations are associated with the electric-dipole−electric-dipole mechanism, the electric-dipole−magnetic-dipole mechanism, the magnetic-dipole−electric-dipole mechanism, and the magnetic-dipole−magnetic-dipole mechanisms. For the near-electronic resonant case, our derivation shows that the band-shape functions of the SFG spectra for the SPP and PPS cases should be the same. For the singly resonant IR−UV SFG case, SSP, SPS, and PPP are due to the contributions from the electric-dipole−magnetic-dipole SFG and/or the magnetic-dipole−electric-dipole SFG. Therefore, their SFG signals should be weaker than those from the electric-dipole−electric-dipole SFG (SPP and PSP). In addition, our theoretical results imply that the selection rules of SSP, SPS, and PPP polarizations are, in principle, different. For the doubly resonant IR SFG case, the SFG intensity difference in solution and on the surface is due to the fact that the former is zero in the electric-dipole−electric-dipole approximation. A nonzero contribution under these polarization conditions indicates that the effect of either the non-Condon effect or the breakdown of the B−O approximation should be involved. We have also taken into account the non-Condon effect and the breakdown of the B−O approximation in our theoretical expressions, and we have shown that the band shapes for these two cases should be different.

Finally, we would like to emphasize that, in this paper, molecular−theoretical expressions for three different types of SFG experiments have been presented; the near-electronic resonance SFG signal is the easiest to compute, because it is electric-dipole allowed and, thus, quantum chemistry calcula-

TABLE 4: Laser and Detection Polarization Combinations for the Doubly Resonant IR−SFG Spectrum of *R*-BN in Acetone Solution[a]

polarization combination, $\eta\eta_1\eta_2$	e−e $\hat{e}_{S\eta}\cdot(\hat{e}_{1\eta_1}\times\hat{e}_{2\eta_2})$	e−m $\hat{e}_{S\eta}\cdot(\hat{e}_{1\eta_1}\times\hat{b}_{2\eta_2})$	m−e $\hat{e}_{S\eta}\cdot(\hat{b}_{1\eta_1}\times\hat{e}_{2\eta_2})$	m−m $\hat{e}_{S\eta}\cdot(\hat{b}_{1\eta_1}\times\hat{b}_{2\eta_2})$
PPP	0	$-\sin(\theta_1-\theta_S)$	$-\sin(\theta_2+\theta_S)$	0
SSS	0	0	0	$-\sin(\theta_1+\theta_2)$
SPS	0	$\sin(\theta_1+\theta_2)$	0	0
PSS	0	$-\sin(\theta_2+\theta_S)$	$-\sin(\theta_1-\theta_S)$	0
SSP	0	0	$-\sin(\theta_1+\theta_2)$	0
SPP	$\sin(\theta_1+\theta_2)$	0	0	0
PPS	$\sin(\theta_1-\theta_S)$	0	0	$-\sin(\theta_2+\theta_S)$
PSP	$-\sin(\theta_2+\theta_S)$	0	0	$\sin(\theta_1-\theta_S)$

[a] Experimental geometry from ref 51 is used.

tions can easily be applied to quantitatively calculate molecular properties that are explicitly given in the theoretical expressions. For the other two cases, they are electric-dipole forbidden and their allowedness can be attributed to the electric-dipole−magnetic-dipole interactions, a non-Condon effect, and the breakdown of the B−O approximation; although the electric-dipole−magnetic-dipole contribution can easily be computed using current quantum chemistry calculation methods, the other two mechanisms require difficult calculations of the vibronic couplings.

Appendix A

We have also derived the molecular−theoretical expressions of SFG for the quadrupole $\vec{Q} = {}^1/_6(3\Sigma_i\, e\vec{r}_i \otimes \vec{r}_i - \Sigma_i\, er_i^2)$ contributions. Because they do not have any significant role in this paper, for comparison, only the resulting expression for the e−Q case is given in the following:

$$\langle S^{e-Q}_{\eta\eta_1\eta_2}(t)\rangle_{env} = \exp[-it(\omega_1+\omega_2)]\frac{iE_1E_2\omega_2}{c}F_{ng}(\omega_1+\omega_2)\times \lfloor L_Q(\hat{e}_S,\hat{e}_{2\eta_2};\hat{e}_{1\eta_1},\hat{k}_2)D_Q^{(1)}(\omega_2)+L_Q(\hat{e}_S,\hat{k}_2;\hat{e}_{1\eta_1},\hat{e}_{2\eta_2})D_Q^{(2)}(\omega_2)\rfloor + \exp[-it(\omega_1+\omega_2)]\frac{iE_1E_2\omega_1}{c}F_{ng}(\omega_1,\omega_2)\lfloor L_Q(\hat{e}_S,\hat{e}_{1\eta_1};\hat{e}_{2\eta_2},\hat{k}_1)\times D_Q^{(1)}(\omega_1)+L_Q(\hat{e}_S,\hat{k}_1;\hat{e}_{1\eta_1},\hat{e}_{2\eta_2})\omega_1 D_Q^{(2)}(\omega_1)\rfloor \quad \text{(A-1)}$$

where

$$L_Q(\hat{e}_S,\hat{e}_{2\eta_2};\hat{e}_{1\eta_1},\hat{k}_2) = \frac{1}{30\hbar^2}(\hat{e}_S\cdot\hat{e}_{2\eta_2})(\hat{e}_{1\eta_1}\cdot\hat{k}_2) \quad \text{(A-2)}$$

$$D_Q^{(1)}(\omega_2) = \sum_{n'}\frac{1}{\omega_{n'g}-\omega_2}[4(\vec{\mu}_{gn}\cdot\vec{Q}_{n'g}\cdot\vec{\mu}_{nn'}) - (\vec{\mu}_{nn'}\cdot\vec{Q}_{n'g}\cdot\vec{\mu}_{gn})] \quad \text{(A-3)}$$

and

$$D_Q^{(2)}(\omega_1) = \sum_{n'}\frac{1}{\omega_{n'g}-\omega_2}[-(\vec{\mu}_{gn}\cdot\vec{Q}_{n'g}\cdot\vec{\mu}_{nn'}) + 4(\vec{\mu}_{nn'}\vec{Q}\cdot_{n'g}\cdot\vec{\mu}_{gn})] \quad \text{(A-4)}$$

If SPP or PPS is chosen, then we have $\langle S^{e-Q}_{\eta\eta_1\eta_2}(t)\rangle_{env} = 0$, whereas if SPS with a $(\hat{e}_{1\eta_1}\cdot\hat{e}_{2\eta_2}) = 1$ configuration is chosen, then we have

$$\langle S^{e-Q}_{\eta\eta_1\eta_2}(t)\rangle_{env} = \exp[-it(\omega_1+\omega_2)]\frac{iE_1E_2\omega_2}{c}\times L_Q(\hat{e}_S,\hat{e}_{2\eta_2};\hat{e}_{1\eta_1},\hat{k}_2)D_Q^{(1)}(\omega_2)F_{ng}(\omega_1+\omega_2) \quad \text{(A-5)}$$

Appendix B

According to the B−O adiabatic approximation, the electronic wave functions $\Phi_n(q,Q)$ and $\Phi_g(q,Q)$ are dependent on not only electronic coordinates q but also nuclear coordinates Q and the dependence of $\Phi_n(q,Q)$ and $\Phi_g(q,Q)$ on Q can be performed as follows. Notice that

$$\hat{H}_e(q,Q)\Phi_a(q,Q) = U_a(Q)\Phi_a(q,Q) \quad \text{(B-1)}$$

and

$$\hat{H}_e(q,0)\Phi_a(q,0) = U_a(0)\Phi_a(q,0) \quad \text{(B-2)}$$

where $\hat{H}_e(q,Q)$ represents the Hamiltonian of electronic motion. Using $\Phi_a(q,0)$ as the basis set, we find, using the perturbation method,

$$\hat{H}_e(q,Q) = \hat{H}_e(q,0) + \sum_p\left(\frac{\partial\hat{H}_e}{\partial Q_p}\right)_p Q_p + \cdots \quad \text{(B-3)}$$

$$\Phi_a(q,Q) = \Phi_a(q,0) + \sum_b^{b\neq a}\frac{\left\langle\Phi_b(q,0)\left|\sum_p\left(\frac{\partial\hat{H}_e}{\partial Q_p}\right)_0 Q_p\right|\Phi_a(q,0)\right\rangle}{U_a(0)-U_b(0)}\times \Phi_b(q,0)+\cdots \quad \text{(B-4)}$$

$$\vec{\mu}_{ng} = \langle\Phi_n(q,Q)|\vec{\mu}|\Phi_g(q,Q)\rangle = \vec{\mu}^0_{ng} + \sum_p\left(\frac{\partial\vec{\mu}_{ng}}{\partial Q_p}\right)_0 Q_p + \cdots \quad \text{(B-5)}$$

and

$$\left(\frac{\partial\vec{\mu}_{ng}}{\partial Q_p}\right)_0 = \sum_b^{b\neq n}\frac{\left\langle\Phi_b(q,0)\left|\left(\frac{\partial\hat{H}_e}{\partial Q_p}\right)_0\right|\Phi_n(q,0)\right\rangle}{U_n(0)-U_b(0)}\vec{\mu}^0_{bg} + \sum_c^{c\neq g}\frac{\left\langle\Phi_c(q,0)\left|\left(\frac{\partial\hat{H}_e}{\partial Q_p}\right)_0\right|\Phi_g(q,0)\right\rangle}{U_g(0)-U_c(0)}\vec{\mu}^0_{nc}+\cdots \quad \text{(B-6)}$$

where $\langle\Phi_b(q,0)|(\partial\hat{H}_e/\partial Q_p)_0|\Phi_n(q,0)\rangle$ and $\langle\Phi_c(q,0)|(\partial\hat{H}_e/\partial Q_p)_0|\Phi_g(q,0)\rangle$ denote the so-called vibronic coupling.

Next, we consider the effect of the B−O coupling $\hat{H}'_{BO}$. According to the B−O approximation,

$$[\hat{T}_n + \hat{H}_e(q,Q)]\psi^0_{av}(q,Q) = E^0_{av}\,\psi^0_{av}(q,Q) \quad \text{(B-7)}$$

and

$$\psi^0_{av}(q,Q) = \Phi_a(q,Q)\Theta_{av}(Q) \quad \text{(B-8)}$$

where $\hat{T}_n$ denotes the kinetic energy operator of nuclear motion. The effect of $\hat{H}'_{BO}$ can be calculated perturbatively (see eqs 4-20

and 4-21). It follows that

$$\vec{\mu}_{gv,nu} = \vec{\mu}^0_{gv,nu} + \sum_{n'u'}^{n'u' \neq gv} \frac{\langle \psi^0_{n'u'} | \hat{H}'_{BO} | \psi^0_{nu} \rangle}{E^0_{nu} - E^0_{n'u'}} \vec{\mu}^0_{gv,n'u'} + \sum_{n''u''}^{n''u'' \neq gv} \sum_{n''u''} \frac{\langle \psi^0_{n''u''} | \hat{H}'_{BO} | \psi^0_{gv} \rangle}{E^0_{gv} - E^0_{n''u''}} \vec{\mu}^0_{n''u'',nu} + \cdots \quad \text{(B-9)}$$

or approximately ($\Phi_a(q,Q) \approx \Phi_a(q,0) \equiv \Phi^0_a$)

$$\vec{\mu}_{gv,nu} = \vec{\mu}^0_{gn} \langle \Theta_{gv} | \Theta_{nu} \rangle + \sum_p \sum_{n'}^{n' \neq n} \frac{\left\langle \Phi^0_n \left| \frac{\partial \hat{H}_e}{\partial Q_p} \right| \Phi^0_{n'} \right\rangle \left\langle \Theta_{gv} \left| - \hbar^2 \frac{\partial \Theta_{nu}}{\partial Q_p} \right. \right\rangle}{\{U_n(0) - U_{n'}(0)\}^2} \vec{\mu}^0_{gn'} + \cdots \quad \text{(B-10)}$$

This should be compared with the non-Condon effect,

$$\vec{\mu}_{gv,nu} = \vec{\mu}^0_{gn} \langle \Theta_{gv} | \Theta_{nu} \rangle + \sum_p \sum_{n'}^{n' \neq n} \frac{\left\langle \Phi^0_n \left| \frac{\partial \hat{H}_e}{\partial Q_p} \right| \Phi^0_{n'} \right\rangle \langle \Theta_{gv} | Q_p | \Theta_{nu} \rangle}{U_n(0) - U_{n'}(0)} \vec{\mu}^0_{gn'} + \cdots \quad \text{(B-11)}$$

Equations B-10 and B-11 show that the $\hat{H}'_{BO}$ contribution is one order of vibronic coupling smaller than that of the non-Condon effect contribution.

Appendix C

To discuss the band-shape function, we shall let

$$F_p(\omega_{IR},\omega_{UV}) = \sum_u \frac{\langle \Theta_{gv'} | Q_p | \Theta_{gv} \rangle}{(\omega_{nu,gv} - i\gamma_{nu,gv} - \omega_{IR} - \omega_{UV})(\omega'_{gv',gv} - i\gamma_{gv',gv} - \omega_{IR})} \times [\langle \Theta_{gv} | Q_p | \Theta_{nu} \rangle \langle \Theta_{nu} | \Theta_{gv'} \rangle - \langle \Theta_{gv} | \Theta_{nu} \rangle \langle \Theta_{nu} | Q_p | \Theta_{gv'} \rangle] \quad \text{(C-1)}$$

For harmonic potential surfaces, we find, in the low-temperature range,

$$F_p(\omega_{IR},\omega_{UV}) = \frac{\sqrt{\frac{1}{2\beta_p}}}{(\omega_p - i\gamma_{g1,g0} - \omega_{IR})} \sum_u \frac{1}{(\omega_{nu,g0} - i\gamma_{nu,g0} - \omega_{IR} - \omega_{UV})} \times [\langle \chi_{g0p} | Q_p | \chi_{nup} \rangle \langle \chi_{nup} | \chi_{g1p} \rangle - \langle \chi_{g0p} | \chi_{nup} \rangle \langle \chi_{nup} | Q_p | \chi_{g1p} \rangle] \times \prod_i^{i \neq p} \left(\frac{S_i^{u_i} \exp(-S_i)}{u_i!} \right) \quad \text{(C-2)}$$

Here, we have assumed that all the oscillators except for the Q_p mode are displaced harmonic oscillators and S_i denotes the Huang−Rhys factor. It follows that

$$F_p(\omega_{IR},\omega_{UV}) = \frac{\sqrt{\frac{1}{2\beta_p}}}{(\omega_p - i\gamma_{g1,g0} - \omega_{IR})} \int_0^\infty dt \exp\{-it(\omega_{nu,gv} - \omega_{IR} - \omega_{UV}) - t\gamma_{nu,gv} + \sum_{i \neq p} [-S_i + S_i \exp(-it\omega_i)]\} \bar{G}_p(t) \quad \text{(C-3)}$$

where

$$\bar{G}_p(t) = \sum_{u_p=0}^{\infty} [\langle \chi_{g0p} | Q_p | \chi_{nup} \rangle \langle \chi_{nup} | \chi_{g1p} \rangle - \langle \chi_{g0p} | \chi_{nup} \rangle \times \langle \chi_{nup} | Q_p | \chi_{g1p} \rangle] \exp\left\{ -it \left[\left(u_p + \frac{1}{2} \right) \omega'_p - \left(\frac{1}{2} \right) \omega_p \right] \right\} \quad \text{(C-4)}$$

and $\bar{G}_p(t)$ can be expressed as

$$\bar{G}_p(t) = \frac{1}{\left(\beta_p + \beta'_p \coth \frac{\lambda'_p}{2} \right)} - \sqrt{2\beta_p{}^2 \beta'_p} \exp\left(\frac{it\omega_p}{2} \right) \exp\left[- \frac{\beta_p \beta'_p d_p{}^2 \tanh \frac{\lambda'_p}{2}}{\beta_p + \beta'_p \tanh \frac{\lambda'_p}{2}} \right] \Bigg/ \sqrt{\left(\beta_p \sinh \frac{\lambda'_p}{2} + \beta'_p \cosh \frac{\lambda'_p}{2} \right) \left(\beta_p \cosh \frac{\lambda'_p}{2} + \beta'_p \sinh \frac{\lambda'_p}{2} \right)} \quad \text{(C-5)}$$

where $Q'_p = Q_p + d_p$, $\beta_p = \omega_p/\hbar$, $\beta'_p = \omega'_p/\hbar$ and $\lambda_p = it\omega'_p$. If $\beta_p = \beta'_p$, then eq C-5 reduces to

$$\bar{G}_p(t) = \frac{-[1 - \exp(-\lambda_p)]}{\sqrt{2\beta_p}} \exp\{-S_p[1 - \exp(-\lambda_p)]\} \quad \text{(C-6)}$$

Next, we consider the SFG band-shape function due to the breakdown of the B−O approximation. Using eq B-11 (see Appendix B), we obtain

$$\vec{\mu}_{gv,nu} \times \vec{\mu}_{nu,gv'} = \sum_{n'u'}^{n'u' \neq nu} \frac{\langle \psi^0_{n'u'} | \hat{H}'_{BO} | \psi^0_{nu} \rangle}{E^0_{nu} - E^0_{n'u'}} (\vec{\mu}^0_{gv,n'u'} \times \vec{\mu}^0_{nu,gv'} + \vec{\mu}^0_{gv,nu} \times \vec{\mu}^0_{n'u',gv'}) + \sum_{n''u''}^{n''u'' \neq gv} \frac{\langle \psi^0_{n''u''} | \hat{H}'_{BO} | \psi^0_{gv} \rangle}{E^0_{gv} - E^0_{n''u''}} (\vec{\mu}^0_{n''u'',nu} \times \vec{\mu}^0_{nu,gv'}) + \sum_{n''u''}^{n''u'' \neq gv'} \frac{\langle \psi^0_{n''u''} | \hat{H}'_{BO} | \psi^0_{gv'} \rangle}{E^0_{gv'} - E^0_{n''u''}} (\vec{\mu}^0_{gv,nu} \times \vec{\mu}^0_{nu,n''u''}) + \cdots \quad \text{(C-7)}$$

We can see from eq C-7 that the SFG band-shape function in this case will be very complicated. In the following, we shall discuss some special cases. If we ignore the contribution from the ground electronic state, eq C-7 reduces to

$$\vec{\mu}_{gv,nu} \times \vec{\mu}_{nu,gv'} = \sum_{n'u'}^{n'u' \neq nu} \frac{\langle \psi^0_{n'u'} | \hat{H}'_{BO} | \psi^0_{nu} \rangle}{E^0_{nu} - E^0_{n'u'}} (\vec{\mu}^0_{gn'} \times \vec{\mu}^0_{ng}) \times [\langle \Theta_{gv} | \Theta_{n'u'} \rangle \langle \Theta_{nu} | \Theta_{gv'} \rangle - \langle \Theta_{gv} | \Theta_{nu} \rangle \langle \Theta_{n'u'} | \Theta_{gv'} \rangle] + \cdots \quad \text{(C-8)}$$

Here, the Condon approximation has been used. For the single-mode case at $T = 0$, we obtain

$$\vec{\mu}_{g_0,nu} \times \vec{\mu}_{nu,g1} = \sum_{n'u'}^{n'u' \neq nu} \frac{\langle \Phi_{n'} \chi_{n'u'p} | \hat{H}'_{BO} | \Phi_n \chi_{nup} \rangle}{E^0_{nu} - E^0_{n'u'}} (\vec{\mu}^0_{gn'} \times \vec{\mu}^0_{ng}) \times [\langle \chi_{g_{0p}} | \chi_{n'u'_p} \rangle \langle \chi_{nu_p} | \chi_{g_{1p}} \rangle - \langle \chi_{g_{0p}} | \chi_{nu_p} \rangle \langle \chi_{n'u'_p} | \chi_{g_{1p}} \rangle] + \cdots \quad \text{(C-9)}$$

where, for a displaced oscillator,

$$\langle \chi_{g_{0p}} | \chi_{nu_p} \rangle = \langle \chi_{g_{0p}}(Q_p) | \chi_{nu_p}(Q'_p) \rangle = \frac{(\sqrt{\beta_p/2} d_p)^{u_p}}{\sqrt{u_p!}} \exp\left(-\frac{\beta_p d_p^2}{4}\right) \quad \text{(C-10)}$$

$$\langle \chi_{n'u'_p} | \chi_{g_{1p}} \rangle = \langle \chi_{n'u'_p}(Q''_p) | \chi_{g1_p}(Q_p) \rangle = \frac{(\sqrt{\beta_p/2} d'_p)^{u'_p - 1}}{\sqrt{u'_p!}} (u'_p - \beta_p d'^2_p/2) \exp\left(-\frac{\beta_p d_p^2}{4}\right) \quad \text{(C-11)}$$

and so on. Here, $Q'_p = Q_p + d_p$ and $Q''_p = Q_p + d'_p$. The multimode case can be treated similarly.

The inhomogeneity effect on the SFG band-shape function can be treated using, for example, $F_p(\omega_1,\omega_2)$, which is given by eq C-3. For the inhomogeneities of the electronic gap ω_{ng}, the distribution function of ω_{ng} is usually assumed to be Gaussian:

$$f(\omega_{ng}) = \frac{1}{\sqrt{\pi D^2}} \exp\left[-\frac{(\omega_{ng} - \bar{\omega}_{ng})^2}{D^2}\right] \quad \text{(C-12)}$$

In this case, $F_p(\omega_1,\omega_2)$ becomes

$$F_p(\omega_{IR},\omega_{UV}) = \frac{\sqrt{\frac{1}{2\beta_p}}}{(\omega_p - i\gamma_{g_1,g_0} - \omega_{IR})} \int_0^\infty dt \times \exp\left[-it(\bar{\omega}_{nu,gv} - \omega_{IR} - \omega_{UV}) - \frac{t^2 D^2}{4} - t\gamma_{nu,gv}\right] \times \exp\{\sum_{i \neq p} [-S_i + S_i \exp(-it\omega_i)]\} \bar{G}_p(t) \quad \text{(C-13)}$$

Acknowledgment. This work was supported by Academia Sinica and National Science Council (Taiwan). One of the authors (M.H.) would also like to thank the NSC for financial support (NSC-92-2113- M-002-041-) and the National Center for High-Performance Computing (Hsinchu, Taiwan) for providing access to the computational resources.

Supporting Information Available: Molecular diagram of the R-BN and S-BN structures, and molecular properties of the fully optimized geometry of R-BN in B3LYP/6-31* (PDF). This material is available free of charge via the Internet at http://pubs.acs.org.

Note Added after ASAP Posting. This paper was posted ASAP on July 24, 2004, with typographical errors in eq 4-2. The corrected version was posted September 20, 2004.

References and Notes

(1) Sandu, C.; Singh, R. K. *Food Technol.* **1991**, *45*, 84.
(2) Hubbell, J. A. *Bio/Technology* **1995**, *13*, 565.
(3) Ishihara, K.; Oshida, H.; Endo, Y.; Ueda, T.; Watanabe, A.; Nakabayashi, N. *J. Biomed. Mater. Res.* **1992**, *26*, 1543.
(4) Martin, B. D.; Gaber, B. P.; Pallerson, C. H.; Turner, D. C. *Langmuir* **1998**, *14*, 3971.
(5) Rechnitz, G. A. *Chem. Eng. News* **1998**, *66*, 24.
(6) Inglis, W.; Sanders, G. H.; Williansm, P. M.; Davies, M. C.; Roberts, C. J.; Tendler, S. J. B. *Langmuir* **2001**, *17*, 7402.
(7) Shen, Y. R. *The Principle of Nonlinear Optics*; Wiley: New York, 1984.
(8) Perrenound-Rinuy, J.; Brevet, P.-F.; Givault, H. H. *Phys. Chem. Chem. Phys.* **2002**, *4*, 4774.
(9) Kim, J.; Somorjai, G. A. *J. Am. Chem. Soc.* **2003**, *125*, 3150.
(10) Shen, Y. R. *Nature* **1989**, *337*, 519.
(11) Shen, Y. R. *Surf. Sci.* **1994**, *229/300*, 551.
(12) Gracia, D. H.; Chen, Z.; Shen, Y. R.; Somorjai, G. A. *Acc. Chem. Res.* **1999**, *32*, 930.
(13) Opdahl, A.; Phillips, R. A.; Somorjai, G. A. *J. Phys. Chem. B* **2002**, *106*, 5212.
(14) Wang, J.; Buck, S. M.; Chen, Z. *J. Phys. Chem. B* **2002**, *106*, 11666.
(15) Lu, Y.; Messmer, M. C. *J. Am. Chem. Soc.* **2002**, *124*, 9714.
(16) Petralli-Mollow, T.; Wong, T. M.; Byers, J. D.; Yee, H. I.; Hicks, J. M. *J. Phys. Chem.* **1993**, *97*, 1383.
(17) Byers J. D.; Hicks, J. M. *Chem. Phys. Lett.* **1994**, *231*, 216.
(18) Belkin, M. A.; Hau, S. H.; Wei, X.; Shen, Y. R. *Phys. Rev. Lett.* **2001**, *87*, 113001.
(19) Champagne, B.; Fischer, P.; Buckinphem, A. D. *Chem. Phys. Lett.* **2000**, *331*, 83.
(20) Adler, E. *Phys. Rev.* **1964**, *134*, A728.
(21) Flytzanis, C. In *Quantum Electronics*; Rabin, H., Tang, C. L., Eds.; Academic Press: New York, 1975; Vol. 1, Part A.
(22) Fischer, P.; Beckwitt, K.; Wise, F. W.; Albrecht, A. C. *Chem. Phys. Lett.* **2002**, *352*, 463.
(23) Fischer, P.; Wise, F. W.; Albrecht, A. C. *J. Phys. Chem. A* **2003**, *107*, 8232.
(24) Lin, S. H.; Hayashi, M.; Islampour, R.; Yu, J.; Yang, D. Y.; Wu, G. Y. C. *Physica B* **1996**, *222*, 191.
(25) Hayashi, M.; Lin, S. H.; Raschke, M. B.; Shen, Y. R.; *J. Phys. Chem. A* **2002**, *106*, 2271.
(26) Rosenfeld, L. *Z. Phys.* **1928**, *42*, 161.
(27) Moffitt, W. *J. Chem. Phys.* **1956**, *25*, 468.
(28) Tinoco, I. *Adv. Chem. Phys.* **1962**, *4*, 113.
(29) Nakanishi, K.; Harada, N. *Circular Dichroism Spectroscopy—Exciton Coupling in Organic Stereochemistry*; University Science Books: Mill Valley, CA, 1983.
(30) Charney, E. *The Molecular Basis of Optical Activity*; Robert E. Krieger Publishing Company: Malabar, FL, 1985.
(31) Condon, E. U. *Rev. Mod. Phys.* **1937**, 432.
(32) Lin, S. H.; Alden, R. G.; Islampour, R.; Ma, H.; Villaeys, A. A. *Density Matrix Method and Femtosecond Processes*; World Scientific: Singapore, 1991; Chapter 1.
(33) Lin, S. H.; Hayashi, M.; Islampour, R.; Yu, J.; Yang, D. Y.; Wu, G. Y. C. *Physica B* **1996**, *222*, 191.
(34) Lin. S. H.; Alden, R. G.; Villaeys, A. A.; Pflumio, V. *Phys. Rev. A* **1993**, *48*, 3137.
(35) Lin, S. H.; Hayashi, M.; Lin, C. H.; Yu, J.; Villaeys, A. A.; Wu, C. Y. C. *Mol. Phys.* **1995**, *84*, 453.
(36) Lin, S. H.; Villaeys, A. A. *Phys. Rev. A* **1994**, *50*, 5134.
(37) Loudon R. *The Quantum Theory of Light*; Oxford University Press: New York, 2001.
(38) Eyring, H.; Walter, J.; Kimball, G. E. *Quantum Chemistry*; Wiley: New York, 1946.
(39) Xing, W.; Hong, S.-C.; Lvovsky, A. I.; Held, H.; Shen, Y. R. *J. Phys. Chem.* **2000**, *104*, 3349.
(40) Craig D. P.; Thirunamachandran T. *Molecular Quantum Electrodynamics*; Academic Press: Orlando, FL, 1984; Chapter 9.
(41) Hayashi, M.; Sugawara, M.; Fujimura, Y. *Phys. Rev. A* **1991**, *43*, 2416.
(42) Yang, P.-K.; Huang, J. Y. *J. Opt. Soc. Am. B* **1998**, *15*, 1698.
(43) Becke, A. D. *J. Chem. Phys.* **1993**, *98*, 5648.
(44) Fischer, P.; Wiersma, D. S.; Righini, R.; Champagne, B.; Buckinphem, A. D. *Phys. Rev. Lett.* **2000**, *85*, 4253.
(45) Frisch, M. J.; Trucks, G. W.; Schlegel, H. B.; Scuseria, G. E.; Robb, M. A.; Cheeseman, J. R.; Montgomery, J. A., Jr.; Vreven, T.; Kudin, K. N.; Burant, J. C.; Millam, J. M.; Iyengar, S. S.; Tomasi, J.; Barone, V.; Mennucci, B.; Cossi, M.; Scalmani, G.; Rega, N.; Petersson, G. A.; Nakatsuji, H.; Hada, M.; Ehara, M.; Toyota, K.; Fukuda, R.; Hasegawa, J.; Ishida, M.; Nakajima, T.; Honda, Y.; Kitao, O.; Nakai, H.; Klene, M.; Li, X.; Knox, J. E.; Hratchian, H. P.; Cross, J. B.; Adamo, C.; Jaramillo, J.; Gomperts, R.; Stratmann, R. E.; Yazyev, O.; Austin, A. J.; Cammi, R.; Pomelli, C.; Ochterski, J. W.; Ayala, P. Y.; Morokuma, K.; Voth, G. A.; Salvador, P.; Dannenberg, J. J.; Zakrzewski, V. G.; Dapprich, S.; Daniels, A. D.; Strain, M. C.; Farkas, O.; Malick, D. K.; Rabuck, A. D.; Raghavachari, K.; Foresman, J. B.; Ortiz, J. V.; Cui, Q.; Baboul, A. G.; Clifford, S.; Cioslowski, J.; Stefanov, B. B.; Liu, G.; Liashenko, A.; Piskorz, P.; Komaromi, I.; Martin, R. L.; Fox, D. J.; Keith, T.; Al-Laham, M. A.; Peng, C. Y.; Nanayakkara, A.; Challacombe, M.; Gill, P. M. W.; Johnson,

B.; Chen, W.; Wong, M. W.; Gonzalez, C.; Pople, J. A. *Gaussian 03*, revision A.1; Gaussian, Inc.: Pittsburgh, PA, 2003.
(46) Belkin, M. A.; Kulakov, T. A.; Ernst, K.-H.; Yan, L.; Shen, Y. R. *Phys. Rev. Lett.* **2000**, *85*, 4474.
(47) Rentzepis, P. M.; Giordmaine, J. A.; Wecht, K. W. *Phys. Rev. Lett.* **1966**, *16*, 792.
(48) Shkurinov, A. P.; Dubrovskii, A. V.; Koroteev, N. I. *Phys. Rev. Lett.* **1993**, *70*, 1085.
(49) Quinet, O.; Champagne, B. J. *Quantum Chem.* **2001**, *85*, 463.
(50) Belkin, M. A.; Shen, Y. R.; Flytzanis, C. *Chem. Phys. Lett.* **2002**, *363*, 479.
(51) Belkin, M. A.; Shen, Y. R. *Phys. Rev. Lett.* **2003**, *91*, 213907-1.